Temperature-dependent quantum pair potentials and their application to dense partially ionized hydrogen plasmas

A. V. Filinov,[1] V. O. Golubnychiy,[1] M. Bonitz,[1] W. Ebeling,[2] and J. W. Dufty[3]
[1]*Institut für Theoretische Physik und Astrophysik, Christian-Albrechts-Universität Kiel, Leibnizstrasse 15, D-24098 Kiel, Germany*
[2]*Institut für Physik, Humboldt-Universität Berlin, Invalidenstrasse 110, D-10115 Berlin, Germany*
[3]*Department of Physics, University of Florida, P.O. Box 118440, Gainesville, Florida 32611-8440, USA*
(Received 28 October 2003; revised manuscript received 25 March 2004; published 28 October 2004)

Extending our previous work [A.V. Filinov *et al.*, J. Phys. A **36**, 5957 (2003)], we present a detailed discussion of accuracy and practical applications of finite-temperature pseudopotentials for two-component Coulomb systems. Different pseudopotentials are discussed: (i) the diagonal Kelbg potential, (ii) the off-diagonal Kelbg potential, (iii) the *improved* diagonal Kelbg potential, (iv) an effective potential obtained with the Feynman-Kleinert variational principle, and (v) the "exact" quantum pair potential derived from the two-particle density matrix. For the *improved* diagonal Kelbg potential, a simple temperature-dependent fit is derived which accurately reproduces the "exact" pair potential in the whole temperature range. The derived pseudopotentials are then used in path integral Monte Carlo and molecular-dynamics (MD) simulations to obtain thermodynamical properties of strongly coupled hydrogen. It is demonstrated that classical MD simulations with spin-dependent interaction potentials for the electrons allow for an accurate description of the internal energy of hydrogen in the difficult regime of partial ionization down to the temperatures of about 60 000 K. Finally, we point out an interesting relationship between the quantum potentials and the effective potentials used in density-functional theory.

DOI: 10.1103/PhysRevE.70.046411 PACS number(s): 52.65.−y, 52.27.Gr, 05.30.−d

I. INTRODUCTION

In recent years, there has been growing interest in the properties of dense *quantum* plasmas, particulary in astrophysics, laser plasmas, and condensed matter; see Refs. [1–7] for an overview. In particular, the thermodynamic properties of hot dense plasmas are essential for the description of plasmas generated by strong lasers [6]. Further, among the phenomena of current interest are the high-pressure compressibility of deuterium [8], metallization of hydrogen [9], and the hypothetical plasma phase transition, e.g. [10–16], which occur in situations where both *interaction and quantum effects* are relevant.

While the case of strong degeneracy and the weak-coupling limit have been extensively studied theoretically, e.g., within the random-phase approximation, plasma properties at *intermediate coupling and degeneracy* (when Γ, the ratio of the potential energy to the mean kinetic energy, exceeds unity) are a hot topic of the present research activity. For an overview of present-day analytical methods, see, e.g., Refs. [2,3,5,14]. Analytical methods typically use a chemical picture where electrons, ions, and bound states (atoms, molecules, etc.) are treated as independent species, and the chemical composition (degree of ionization) is computed from a mass action law (nonideal Saha equation). However, these methods are based on perturbation expansions in the coupling strength and are thus limited to regions of small-coupling parameters, $\Gamma<1$ or $\mathbf{r}_s<1$ ($\mathbf{r}_s$ is the quantum coupling parameter, $\mathbf{r}_s=\overline{\mathbf{r}}/a_B$). Furthermore, the mass action law becomes increasingly inaccurate in the region where the electrons are degenerate (because of uncertainty in the mass action constants). Also, during rapid pressure ionization around the Mott density, the distinction between free and bound particles is an open problem.

On the other hand, in the past decade, static properties (e.g., equation of state) of dense hydrogen in thermal equilibrium have been successfully investigated with "exact" quantum-statistical methods, such as the path integral Monte Carlo (PIMC) method [17–20]. This first-principles numerical technique is well suited for an accurate treatment of many-particle correlation effects in quantum systems, but unfortunately does not give dynamical characteristics of the plasma (with the exception of those obtained within linear-response theory). The alternative numerical approach for dense partially ionized plasmas (which does not have the above shortcoming) is a group of methods based upon *ab initio* quasiclassical molecular-dynamic simulations (MD), e.g., Refs. [21,22], when a real quantum system is projected onto a classical one where most of the quantum effects are included in some effective interparticle interaction potentials [23,24], such as the ones proposed by Kelbg [25], Deutsch [26], Klakow, Toepffer, and Reinhard [21], and many others, e.g., [27–29]. These potentials can be derived from the two-particle Slater sum using Morita's method.

However, no rigorous comparison of the accuracy of these potentials has been done yet, which is one of the aims of this paper. Different quantum potentials are compared with an "exact" pair potential obtained from the two-particle density matrix. Furthermore, we introduce pair potentials including particle statistics, e.g., describing interaction between electrons in the singlet and triplet states, and we use them in our MD simulations of two-component hydrogen plasmas.

This paper is organized as follows. In Sec. II, we discuss different methods to obtain an effective quantum pair potential. In the weak-coupling limit, this potential leads exactly to the off-diagonal Kelbg potential, the properties of which are discussed and compared to its commonly used diagonal ap-

proximation. We outline two methods for a direct solution of the off-diagonal two-body Bloch equation, which are then used in Sec. III for numerical comparison with the Kelbg and improved Kelbg potentials for rigorous assessment of the accuracy of the latter. Further, in Sec. IV we present an analysis of the accuracy of the diagonal and off-diagonal Kelbg potentials in the PIMC simulations. Section V describes an application of the improved Kelbg potentials to classical molecular-dynamics simulations of dense hydrogen. Comparing the results to those of PIMC simulations allows us to conclude that use of the improved Kelbg potential allows us to significantly extend the range of applicability of classical MD to the region of partial ionization and to temperatures as low as approximately one-third of the binding energy. Section VI discusses another field of potential applicability of the quantum potentials, namely density-functional theory. Finally, Sec. VII concludes the paper.

II. EFFECTIVE QUANTUM PAIR POTENTIALS

In this section, we discuss different possibilities for obtaining effective quantum potentials describing interactions in the two-particle problem.

A. Analytical solution of two-body Bloch equation: Off-diagonal and diagonal Kelbg potential

The equilibrium pair density matrix at a given inverse temperature $\beta=1/k_BT$ is the solution of the two-particle Bloch equation,

$$\frac{\partial}{\partial\beta}\rho(\mathbf{r}_i,\mathbf{r}_j,\mathbf{r}_i',\mathbf{r}_j';\beta)=-\hat{H}\rho(\mathbf{r}_i,\mathbf{r}_j,\mathbf{r}_i',\mathbf{r}_j';\beta),$$

$$\hat{H}=\hat{K}_i+\hat{K}_j+\hat{U}(\mathbf{r}_i,\mathbf{r}_j,\mathbf{r}_i',\mathbf{r}_j'). \tag{1}$$

Numerical methods to obtain the density matrix of Eq. (1) will be considered in Sec. II C. Here, we concentrate on the available analytical solutions in the limit of weak coupling. If the interaction is weak, Eq. (1) can be solved by perturbation theory with the following representation for the two-particle density matrix:

$$\rho_{ij}=\frac{(m_im_j)^{3/2}}{(2\pi\hbar\beta)^3}\exp\left[-\frac{m_i}{2\hbar^2\beta}(\mathbf{r}_i-\mathbf{r}_j')^2\right]\times\exp\left[-\frac{m_j}{2\hbar^2\beta}(\mathbf{r}_i-\mathbf{r}_j')^2\right]\exp[-\beta\Phi_{ij}], \tag{2}$$

where i,j are particle indices, $\rho_{ij}\equiv\rho(\mathbf{r}_i,\mathbf{r}_j,\mathbf{r}_i',\mathbf{r}_j';\beta)$, and $\Phi_{ij}\equiv\Phi(\mathbf{r}_i,\mathbf{r}_j,\mathbf{r}_i',\mathbf{r}_j';\beta)$ is the off-diagonal two-particle effective potential. In the following, we will consider application of this result to Coulomb systems. As a result of first-order perturbation theory, we get explicitly

$$\Phi^0(\mathbf{r}_{ij},\mathbf{r}_{ij}',\beta)\equiv\mathbf{q}_i\mathbf{q}_j\int_0^1\frac{d\alpha}{d_{ij}(\alpha)}\mathrm{erf}\left(\frac{d_{ij}(\alpha)/\lambda_{ij}}{2\sqrt{\alpha(1-\alpha)}}\right), \tag{3}$$

where $d_{ij}(\alpha)=|\alpha\mathbf{r}_{ij}+(1-\alpha)\mathbf{r}_{ij}'|$, $\mathrm{erf}(\mathbf{x})$ is the error function, $\mathrm{erf}(\mathbf{x})=(2/\sqrt{\pi})\int_0^{\mathbf{x}}dte^{-t^2}$, and $\lambda_{ij}^2=\hbar^2\beta/2\mu_{ij}$ with $\mu_{ij}^{-1}=m_i^{-1}+m_j^{-1}$. The diagonal element ($\mathbf{r}_{ij}'=\mathbf{r}_{ij}$) of Eq. (3) is the potential derived by Kelbg and co-workers [4,25],

$$\Phi^0(\mathbf{x}_{ij})=\frac{\mathbf{q}_i\mathbf{q}_j}{\lambda_{ij}\mathbf{x}_{ij}}\{1-e^{-\mathbf{x}_{ij}^2}+\sqrt{\pi}\mathbf{x}_{ij}[1-\mathrm{erf}(\mathbf{x}_{ij})]\} \tag{4}$$

with $\mathbf{x}_{ij}=|\mathbf{r}_{ij}|/\lambda_{ij}$. The Kelbg potential is finite at zero distance, reflecting that it captures the basic quantum diffraction effects and the quantum nature of two-particle interaction at small distances, which prevents any divergence. From Eq. (4), it is also clear that quantum effects become dominant (and the quantum potential deviates from the classical Coulomb potential) at distances $\mathbf{r}_{ij}\lesssim\lambda_{ij}$ given by the thermal deBroglie wavelength. We will see below that, in interacting systems, this is only a rough approximation, and at strong coupling, the expression for the quantum particle "extension" deviates strongly from λ_{ij} and needs to be generalized.

To obtain a simplified expression for the rather complex quantum potential (3), one can approximate the off-diagonal matrix elements by the diagonal ones. A first possibility is to approximate the integral over α by the length of the interval multiplied with the integrand in the center (Mittelwertsatz) which leads to the so-called KTR potential due to Klakow, Toepffer, and Reinhard, which (in the diagonal approximation) is often used in quasiclassical MD simulations [21],

$$\Phi^0(\mathbf{r}_{ij},\mathbf{r}_{ij}',\beta)\equiv\frac{\mathbf{q}_i\mathbf{q}_j}{d_{ij}(1/2)}\mathrm{erf}\left(\frac{d_{ij}(1/2)}{\lambda_{ij}}\right), \tag{5}$$

where $d_{ij}(1/2)=\frac{1}{2}|\mathbf{r}_{ij}+\mathbf{r}_{ij}'|$. Alternatively, the integral can be simplified by taking the off-diagonal Kelbg potential only at the center coordinate,

$$\Phi^0(\mathbf{r}_{ij},\mathbf{r}_{ij}',\beta)\approx\Phi_{ij}^0\left(\frac{|\mathbf{r}_{ij}|+|\mathbf{r}_{ij}'|}{2},\beta\right). \tag{6}$$

Many authors use the *end-point* approximation (4) for the effective potential $\Phi(\mathbf{r}_{ij},\mathbf{r}_{ij}',\beta)$ in the pair density matrix (2) due to the fact that it is very convenient computationally. The pair potential for interparticle interaction is simply replaced by an effective potential which has only a dependence on the radial variables $|\mathbf{r}_{ij}|$, $|\mathbf{r}_{ij}'|$. However, most of the accuracy is usually lost in this end-point approximation.

Since the Kelbg potential is obtained by first-order perturbation theory, its application is limited to weak coupling, $\Gamma\lesssim1$, where Γ is the ratio of mean potential to kinetic energy. In unbound and bound states of an electron-proton pair, this results in the following conditions on temperature:

$$\Gamma=\frac{e^2}{\mathbf{r}}\Big/k_BT\lesssim1\Rightarrow k_BT\gtrsim\frac{e^2}{\mathbf{r}},$$

$$\Gamma=\mathrm{Ry}/k_BT\lesssim1\Rightarrow k_BT\gtrsim\mathrm{Ry}, \tag{7}$$

where $\mathrm{Ry}=\mathrm{Ha}/2=e^2/2a_B$, and a_B is the Bohr radius. For the last case, the Kelbg potential (and any of the simplifying approximations) can be valid only for temperatures sufficiently above the atomic binding energy, i.e., for the case of hydrogen, $T\gtrsim\mathrm{Ry}/k_B\approx158\,000$ K. We address this point in more detail in Sec. IV, where "exact" binding energies and pair correlation functions for an electron-proton pair are

compared with the results obtained with the potentials (3) and (4).

B. Improved diagonal Kelbg potential

The limitation of the Kelbg potential to describe quantum systems only when there are no bound states has led several researchers [1,30,31] to introduce and investigate a more generalized form of the quantum potential with an additional free parameter γ_{ij},

$$\Phi(\mathbf{r}_{ij},\beta)=\frac{\mathbf{q}_i\mathbf{q}_j}{\mathbf{r}_{ij}}\left\{1-e^{-\mathbf{r}_{ij}^2/\lambda_{ij}^2}+\sqrt{\pi}\frac{\mathbf{r}_{ij}}{\lambda_{ij}\gamma_{ij}}\left(1-\mathrm{erf}\left[\gamma_{ij}\frac{\mathbf{r}_{ij}}{\lambda_{ij}}\right]\right)\right\}. \tag{8}$$

This potential has the advantage of preserving the correct first derivative at $\mathbf{r}=0$ of the original Kelbg potential, $\Phi(0,\beta)'_{\mathbf{r}}=-\mathbf{q}_i\mathbf{q}_j/\lambda_{ij}^2$, but at the same time allows the correction of the height of the Kelbg potential at $\mathbf{r}=0$, i.e., $\Phi(0,\beta)=\mathbf{q}_i\mathbf{q}_j\sqrt{\pi}/(\lambda_{ij}\gamma_{ij})$ to include bound states. Using the definition of the effective potential as

$$e^{-\beta\Phi_{ij}}\equiv S_{ij}, \tag{9}$$

where $S_{ij}\equiv S(\mathbf{r}_{ij},\beta)$ is the exact binary Slater sum of particles i,j. The fit parameter γ_{ij} in Eq. (8) is related to the Slater sum at zero interparticle distance according to

$$\gamma_{ij}=-\frac{\sqrt{\pi}}{\lambda_{ij}}\frac{\mathbf{q}_i\mathbf{q}_j\beta}{\ln[S_{ij}(\mathbf{r}_{ij}=0,\beta)]}. \tag{10}$$

It is important to note that γ_{ij} depends both on the temperature and the type of particles. For example, the binary Slater sum of two electrons at zero separation has the form (including the average "$\langle\cdots\rangle$" over possible values of the total spin $S=0,\ 1$)

$$S_{ee}^{\langle\rangle}(\mathbf{r}_{ee}=0,\beta)=2\sqrt{\pi}\xi_{ee}J_1(\xi_{ee}),$$

$$J_1(\xi_{ij})=\int_0^\infty e^{-\mathbf{x}^2}\frac{\mathbf{x}\,d\mathbf{x}}{1-\exp\left(-\dfrac{\pi\xi_{ij}}{\mathbf{x}}\right)}, \tag{11}$$

where the interaction parameter $\xi_{ij}=\mathbf{q}_i\mathbf{q}_j\beta/\lambda_{ij}$.

On the other hand, for an electron-proton pair the Slater sum can be written as

$$S_{ep}(\mathbf{r}_{ep}=0,\beta)=4\sqrt{\pi}\xi_{ep}J_1(\xi_{ep})+\sqrt{\pi}\xi_{ep}^3Z_3(\xi_{ep}),$$

$$Z_n(\xi)=\sum_{y=1}^{\infty}y^{-n}e^{\xi^2/4y^2}, \tag{12}$$

where the last term shows the contribution of the bound states.

The original Kelbg potential was derived for very high temperatures without taking into account exchange between particles. This work was followed by several studies where the pseudopotentials for identical particles have been calculated numerically [32,33] or analytically [34–36] using expansions in a quantum parameter, small-particle separation, and temperature. In the present work, following these studies, we approach the problem of the pseudopotential with exchange by using the formalism of two-particle density matrices (DM). The pair DM can be calculated numerically (see Sec. II C) or expressed in analytical form (2) using the improved Kelbg potential (8).

In the case of a pair of electrons, they can be in a singlet or triplet state, and the spatial wave function is symmetric or antisymmetric under the exchange of particle indices. Thus, one can define a binary effective electron-electron interaction for three different cases,

$$e^{-\beta U_{ij}^{S(T)}}=\frac{\rho^{[2]}(\mathbf{r}_i,\mathbf{r}_j,\mathbf{r}_i,\mathbf{r}_j;\beta)\pm\rho^{[2]}(\mathbf{r}_i,\mathbf{r}_j,\mathbf{r}_j,\mathbf{r}_i;\beta)}{\rho^{[1]}(\mathbf{r}_i,\mathbf{r}_i;\beta)\rho^{[1]}(\mathbf{r}_j,\mathbf{r}_j)},$$

$$e^{-\beta U_{ij}^{\langle\rangle}}=\tfrac{3}{4}e^{-\beta U_{ij}^{T}}+\tfrac{1}{4}e^{-\beta U_{ij}^{S}}, \tag{13}$$

where $\rho^{[1]}$ and $\rho^{[2]}$ are the one- and two-particle density matrices, and U_{ij}^{S}, U_{ij}^{T}, and $U_{ij}^{\langle\rangle}$ are the effective interactions in the singlet state (S), triplet state (T), and the spin-averaged potential, respectively.

If we now approximate the two-particle DM, $\rho^{[2]}$, by Eq. (2) and factorize it into the DM's of the center-of-mass and relative coordinates [the corresponding expressions are given in Sec. II C, cf. Eq. (27)], then we obtain for the pseudopotential between two electrons being in the singlet (triplet) state and for the spin-averaged potential, respectively,

$$U_{ee}^{S(T)}=-\frac{1}{\beta}\ln(e^{-\beta U_{ee}(\mathbf{r},\mathbf{r})}\pm e^{-\mathbf{r}^2/\lambda_{ee}^2}e^{-\beta U_{ee}(\mathbf{r},-\mathbf{r})}), \tag{14}$$

$$U_{ee}^{\langle\rangle}=-\frac{1}{\beta}\ln\left(e^{-\beta U_{ee}(\mathbf{r},\mathbf{r})}-\tfrac{1}{2}e^{-\mathbf{r}^2/\lambda_{ee}^2}e^{-\beta U_{ee}(\mathbf{r},-\mathbf{r})}\right). \tag{15}$$

In this expression, the function, $U_{ee}(\mathbf{r},\mathbf{r}')$, is a pseudopotential between distinguishable particles (i.e., calculated without exchange effects). Thus, one can substitute the original Kelbg potential, Eq. (4), the improved Kelbg potential, Eq. (8), or any further improved approximation for the binary interaction. In the case of two electrons, if we use the improved Kelbg potential (8) for $U_{ee}(\mathbf{r},\mathbf{r})$, then the fit parameter γ_{ee} must be obtained from Eq. (10), where for the binary Slater sum one should take the two distinguishable particles with the Coulomb repulsion case,

$$S_{ee}^{\text{no exc}}(\mathbf{r}_{ee}=0,\beta)=4\sqrt{\pi}\xi_{ee}J_1(\xi_{ee}). \tag{16}$$

It follows from Eq. (15) that an exchange contribution (effect of particle statistics in the pair interaction) arises from the kinetic energy part of the density matrix and the nondiagonal potential, $U_{ee}(\mathbf{r},-\mathbf{r})$, which in the first order of the perturbation theory can be calculated using Eq. (3). A further simplification (which is crucial for the application of the pseudopotentials in semiclassical MD simulations presented in Sec. V) can be achieved by approximating the off-diagonal potential by the diagonal terms, $U_{ee}(\mathbf{r},-\mathbf{r})\approx\frac{1}{2}[U_{ee}(\mathbf{r},\mathbf{r})+U_{ee}(-\mathbf{r},-\mathbf{r})]=U_{ee}(\mathbf{r},\mathbf{r})$. Then the above expressions are reduced to

$$U_{ee,0}^{S(T)} = U_{ee}(\mathbf{r},\mathbf{r}) - \frac{1}{\beta}\ln\{1 \pm e^{-\mathbf{r}^2/\lambda_{ee}^2}\}, \tag{17}$$

$$U_{ee,0}^{\langle\rangle} = U_{ee}(\mathbf{r},\mathbf{r}) - \frac{1}{\beta}\ln\left\{1 - \frac{1}{2}e^{-\mathbf{r}^2/\lambda_{ee}^2}\right\}. \tag{18}$$

We note that in the diagonal approximation for the potential, the exchange term corresponds to the case of the ideal Fermi gas (i.e., exchange without interaction); the exchange term arising from the interaction is missing.

Taking in Eq. (17) the limit $\mathbf{r}\to 0$, we see that the potential of the triplet state shows a logarithmic divergency,

$$U_{ee,0}^{T} = U_{ee}(\mathbf{r},\mathbf{r}) - 2k_BT\ln\left\{\frac{\mathbf{r}}{\lambda_{ee}}\right\} + O\left(\frac{\mathbf{r}^2}{\lambda_{ee}^2}\right), \tag{19}$$

whereas the singlet and the spin-averaged potential acquires an additional exchange contribution,

$$U_{ee,0}^{S,\langle\rangle} = U_{ee}(\mathbf{r},\mathbf{r}) \mp k_BT\ln\{2\} + O\left(\frac{\mathbf{r}^2}{\lambda_{ee}^2}\right), \tag{20}$$

but the slope of these potentials at the origin is the same as in the case without exchange. This means, in the case of Coulomb interaction, the slope is defined by the slope of the original Kelbg potential Φ^0,

$$U_{ee}(\mathbf{r},\mathbf{r})_{\mathbf{r}\to 0} = \Phi_{ee}^0(0) - \frac{e^2\mathbf{r}}{\lambda_{ee}^2} + O\left(\frac{\mathbf{r}^2}{\lambda_{ee}^2}\right). \tag{21}$$

In our previous paper [1], we reported on the temperature dependence of the fitting parameter γ_{ij} for the electron-electron and electron-proton interactions. There, two types of calculations have been presented. The values of $\gamma(\beta)$ were obtained, first, by a least-square fit of the improved diagonal Kelbg potential (IDKP), Eq. (8), to the "exact" pair potential U [see Eq. (27)], and second, from Eq. (10) by evaluating the values of the binary Slater sums. It has been found that both methods agree within statistical uncertainty.

Extending our earlier results, we now present a Padé approximation which contains an analytical temperature dependence of the parameters γ_{ij} which will be useful for practical applications,

$$\gamma_{ep}(T) = \frac{\mathbf{x}_1 + \mathbf{x}_1^2}{1 + a_{ep}\,\mathbf{x}_1 + \mathbf{x}_1^2}, \tag{22}$$

$$\gamma_{ee}(T) = \frac{\gamma_{ee}(T\to 0) + a_{ee}\mathbf{x}_1 + \mathbf{x}_1^2}{1 + \mathbf{x}_1^2}, \tag{23}$$

where $\mathbf{x}_1 = \sqrt{8\pi k_BT/\mathrm{Ha}}$ (with the Hartree energy Ha=2 Ry =315 775 K), $a_{ep}=1.090(14)$, and $a_{ee}=0.18(1)$. The limit value, $\gamma_{ee}(T\to 0)$, has been obtained from Eq. (10) by evaluating the zero-temperature limit of the binary Slater sum (16),

$$\gamma_{ee}(T\to 0) \approx -\frac{2}{\sqrt{\pi}}\tilde{\mathbf{x}}^3\frac{1}{\ln\{8\tilde{\mathbf{x}}^4/\sqrt{\pi}\} - 3\tilde{\mathbf{x}}^2}, \tag{24}$$

with $\tilde{\mathbf{x}} = (|\pi\xi_{ee}|/2)^{1/3}$. The excellent accuracy of the Padé approximation is demonstrated in Fig. 1.

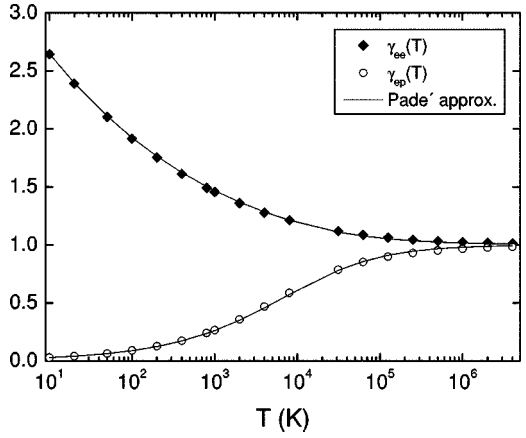

FIG. 1. Temperature dependence of the fit parameter for the binary interactions: electron-proton, $\gamma_{ep}(T)$, and electron-electron (no exchange), $\gamma_{ee}(T)$. Symbols show the γ values obtained with the least-square fit of the IDKP to the "exact" pair potential without exchange. Solid curves correspond to the Padé approximation (22) and (23).

In Fig. 1, we present the temperature dependence of γ obtained from the least-square fit (full and open symbols) to the "exact" pair potential of distinguishable particles (no exchange) and the Padé approximation (22) (solid curves). The most important result is that the corrected Kelbg potential is now *not limited to weak coupling* as is the original Kelbg potential. For the case $\gamma_{ij}=1$, Eq. (8) coincides with Eq. (4). One clearly sees the deviation of γ_{ij} from unity for $T \leqslant 10^6$ K, which shows that the quantum extension of particles has started to be influenced by interaction effects and is now of the order of $\tilde{\lambda}_{ij}=\lambda_{ij}\gamma_{ij}$, instead of the original thermal deBroglie wavelength λ_{ij}. Thus, with the Padé formulas (22) and (23), we have obtained an analytical fit for the quantum extension of the scattering particles.

The Padé approximations (22) and (23) have been successfully used in quasiclassical molecular-dynamics simulations of two-component hydrogen plasmas. As we show in Sec. V, they enable accurate results for partial hydrogen (or other quantum systems of oppositely charged particles with bound states).

Finally, we note that, in the MD simulations of quantum plasmas, it can be advantageous to have spin-dependent potentials for the electron subsystem defined by Eq. (14) or Eq. (17). The spin-resolved approximation allows for refined modeling; for example, it allows for the description of molecule formation, spin density waves, spin-flip processes in the presence of a magnetic field, and so on.

C. Effective potentials from numerical solution of the two-body Bloch equation

In this section, we briefly describe the numerical methods which have been used to solve the two-particle problem in order to obtain the "exact" quantum pair potentials. These results have been used to obtain the analytical fit in the improved Kelbg potential. Furthermore, they will be used to test the accuracy of various analytical approximations for the quantum pair potentials in Sec. III below.

Let us factorize the full two-particle density matrix into a center-of-mass (c.m.) term and a density matrix of relative coordinates,

$$\rho(\mathbf{r}_i,\mathbf{r}_j,\mathbf{r}_i',\mathbf{r}_j';\beta) = \rho_{\text{c.m.}}(\mathbf{R},\mathbf{R}';\beta)\rho(\mathbf{r},\mathbf{r}';\beta), \tag{25}$$

where $\mathbf{R}=(m_i\mathbf{r}_i+m_j\mathbf{r}_j)/(m_i+m_j)$, and $\mathbf{r}=\mathbf{r}_i-\mathbf{r}_j$, and analogously for $\mathbf{R}',\mathbf{r}'$. For the relative DM in analogy with Eq. (2), we define the effective pair potential as

$$\rho(\mathbf{r},\mathbf{r}';\beta) = \rho_{\text{kin}}(\mathbf{r},\mathbf{r}';\beta)e^{-\beta U(\mathbf{r},\mathbf{r}';\beta)}, \tag{26}$$

which results in the following expression:

$$U(\mathbf{r},\mathbf{r}';\beta) = -\frac{1}{\beta}\ln[\rho(\mathbf{r},\mathbf{r}';\beta)/\rho_{\text{kin}}(\mathbf{r},\mathbf{r}';\beta)], \tag{27}$$

where $\rho(\mathbf{r},\mathbf{r}';\beta)_{\text{kin}}$ is the kinetic energy DM.

One of the possibilities to get the relative density matrix $\rho(\mathbf{r},\mathbf{r}';\beta)$ is to directly solve the corresponding one-particle Schrödinger equation and calculate the DM as a contribution from bound and continuum states. This procedure is advantageous when the Schrödinger equation can be solved analytically and we know analytical expressions for contributions of scattering and bound states, as, for example, for the Coulomb potential, e.g., [36]. But if that is not the case, a separate calculation of each matrix element for each new value of end points $\mathbf{r}$ and $\mathbf{r}'$ will be required, which is not efficient and a time-demanding procedure. In principle, such calculations can be done in advance with $U(\mathbf{r},\mathbf{r}';\beta)$ stored in the tables of the potential, but one still needs to solve the Schrödinger equation many times for each value of quantum numbers and also for wave functions of continuum states.

It is possible to approach this problem from the other side and calculate the DM directly without solving the Schrödinger equation. In this work, we apply two efficient methods, namely the *matrix squaring technique* [32,37] and the Feynman-Kleinert *variational approach* [38,39]. In Sec. III, we will compare the accuracy of the pseudopotentials obtained with these methods.

1. Matrix squaring technique

The exact off-diagonal pair density matrix can be calculated efficiently by the method introduced by Storer and Klemm [32]. For the case of spherical symmetry of the interaction potential, the relative pair density matrix in Eq. (25) is expanded in terms of partial waves. This expansion reads, for the two- and three-dimensional cases,

$$\rho^{\text{2D}}(\mathbf{r},\mathbf{r}';\beta) = \frac{1}{2\pi\sqrt{\mathbf{r}\,\mathbf{r}'}}\sum_{l=-\infty}^{+\infty}\rho_l(\mathbf{r},\mathbf{r}';\beta)e^{il\Theta},$$

$$\rho^{\text{3D}}(\mathbf{r},\mathbf{r}';\beta) = \frac{1}{4\pi\mathbf{r}\,\mathbf{r}'}\sum_{l=0}^{+\infty}(2l+1)\times\rho_l(\mathbf{r},\mathbf{r}';\beta)P_l(\cos\Theta), \tag{28}$$

where Θ is the angle between $\mathbf{r}$ and $\mathbf{r}'$. Each partial-wave component satisfies the 1D Bloch equation for a single particle in an external potential given by the interaction potential and also a convolution equation,

$$\rho_l(\mathbf{r},\mathbf{r}';\tau) = \int_0^\infty d\mathbf{r}''\,\rho_l(\mathbf{r},\mathbf{r}'';\tau/2)\rho_l(\mathbf{r}'',\mathbf{r}';\tau/2). \tag{29}$$

This is the basic equation of the *matrix-squaring method* which allows the calculation of the function ρ_l at a given temperature $1/\tau$ from the same function at a temperature twice as high. Squaring the density matrix k times results in a lowering of the temperature by a factor of 2^k. Each squaring involves only a one-dimensional integration which, due to the Gaussian-like nature of the integrand in Eq. (29), can be performed quite accurately and efficiently by standard numerical procedures. To start the matrix-squaring iterations, Eq. (29), one needs a known accurate high-temperature form for the density matrix. A convenient choice is the semiclassical approximation,

$$\rho_l(\mathbf{r},\mathbf{r}';\tau) = \rho_l^0(\mathbf{r},\mathbf{r}';\tau)\times\exp\left(-\frac{\tau}{|\mathbf{r}-\mathbf{r}'|}\int_{\mathbf{r}}^{\mathbf{r}'}V(\mathbf{x})d\mathbf{x}\right), \tag{30}$$

where $\rho_l^0(\mathbf{r},\mathbf{r}';\tau)$ is the partial-wave component of the free-particle density matrix.

Once the pair density matrix $\rho_l(\mathbf{r},\mathbf{r}';\tau)$ is computed for the desired value of τ, it is substituted into Eqs. (28) and (29), and a summation over partial waves readily yields the full relative density matrix.

2. Variational perturbation approach

As a second method for solving the off-diagonal Bloch equation, we used the *variational perturbation expansion* developed by Feynman and Kleinert [38]. In this procedure, the initial density matrix is presented in the form of a trial path integral which consists of a suitable superposition of local harmonic-oscillator path integrals centered at arbitrary average positions $\mathbf{x}_m$, each with its own frequency squared $\Omega^2(\mathbf{x}_m)$. One starts from decomposing the action in the density matrix as

$$\rho(\mathbf{r},\mathbf{r}';\beta) = \int_{(\mathbf{r},0)\to(\mathbf{r}',\hbar\beta)}\mathcal{D}\mathbf{x}\,e^{-A[\mathbf{x}]/\hbar}, \tag{31}$$

$$A[\mathbf{x}] = A_{\Omega,\mathbf{x}_m}[\mathbf{x}] + A_{\text{int}}[\mathbf{x}], \tag{32}$$

with $A_{\Omega,\mathbf{x}_m}[\mathbf{x}]$ being the action of a trial harmonic oscillator with the potential minimum located at $\mathbf{x}_m$, and $\mathcal{D}$ being the functional integral over all trajectories. The interaction part

$$A_{\text{int}}[\mathbf{x}] = \int_0^{\hbar\beta}d\eta\left[V[\mathbf{x}(\eta)] - \tfrac{1}{2}\mu\,\Omega^2[\mathbf{x}(\eta)-\mathbf{x}_m]^2\right], \tag{33}$$

is defined as the difference between the original potential $V(\mathbf{x})$ and the displaced harmonic oscillator. The Ω^2 term in Eq. (33) compensates for the contribution of $A_{\Omega,\mathbf{x}_m}[\mathbf{x}]$ in Eq. (32). Now one can calculate the density matrix (31) by treating the interaction (33) as a perturbation, leading to a moment expansion

$$\rho(\mathbf{r},\mathbf{r}';\beta)=\rho_0^{\Omega,\mathbf{x}_m}(\mathbf{r},\mathbf{r}';\beta)\left(1-\frac{1}{\hbar}\langle A_{\rm int}[\mathbf{x}]\rangle_{\mathbf{r},\mathbf{r}'}^{\Omega,\mathbf{x}_m}+\frac{1}{2\hbar^2}\langle A_{\rm int}^2[\mathbf{x}]\rangle_{\mathbf{r},\mathbf{r}'}^{\Omega,\mathbf{x}_m}-\cdots\right)$$
$$=e^{-\tau W_N^{\Omega,\mathbf{x}_m}}\left(\frac{\mu}{2\pi\hbar^2\tau}\right)^{d/2}, \tag{34}$$

with the definition

$$W_N^{\Omega,\mathbf{x}_m}=\frac{d}{2\beta}\ln\frac{\sinh\hbar\beta\Omega}{\hbar\beta\Omega}+\frac{\mu\Omega}{2\hbar\beta\sinh\hbar\beta\Omega}\times[(\tilde{\mathbf{r}}^2+\tilde{\mathbf{r}}'^2)\cosh\hbar\beta\Omega-2\tilde{\mathbf{r}}\tilde{\mathbf{r}}']-\frac{1}{\beta}\sum_{n=1}^{N}\frac{(-1)^n}{n!\,\hbar^n}\langle A_{\rm int}[\mathbf{x}]\rangle_{\mathbf{r},\mathbf{r}'}^{\Omega,\mathbf{x}_m}, \tag{35}$$

where d is the space dimensionality and N the order of the approximation. The function $\rho_0^{\Omega,\mathbf{x}_m}(\mathbf{r},\mathbf{r}')$ is the trial harmonic-oscillator density matrix, $\tilde{\mathbf{r}}=(\mathbf{r}-\mathbf{x}_m)$, $\tilde{\mathbf{r}}'=(\mathbf{r}'-\mathbf{x}_m)$, and the expectation value of the interaction action on the right-hand side of Eq. (35) is given by

$$\langle A_{\rm int}^n[\mathbf{x}]\rangle_{\mathbf{r},\mathbf{r}'}^{\Omega,\mathbf{x}_m}=\frac{1}{\rho_0^{\Omega,\mathbf{x}_m}(\mathbf{r},\mathbf{r}')}\int_{\tilde{\mathbf{r}},0}^{\tilde{\mathbf{r}}',\hbar\beta}\mathcal{D}\tilde{\mathbf{x}}\prod_{l=1}^{n}\left\{\int_0^{\hbar\beta}d\tau_l\times V_{\rm int}[\tilde{\mathbf{x}}(\tau_l)+\mathbf{x}_m]e^{\{-(1/\hbar)A_{\Omega,\mathbf{x}_m}[\tilde{\mathbf{x}}+\mathbf{x}_m]\}}\right\}. \tag{36}$$

The function $W_N^{\Omega,\mathbf{x}_m}$ can be identified as an *effective quantum potential* which is to be optimized with respect to the variational parameters $\{\Omega^2(\mathbf{r},\mathbf{r}';\beta),\mathbf{x}_m(\mathbf{r},\mathbf{r}';\beta)\}$. Note that, in the high-temperature limit, this effective potential goes over to the original potential $V(\mathbf{r})$. The optimal parameter values are determined from the extremity conditions

$$\frac{\partial W_N^{\Omega,\mathbf{x}_m}(\mathbf{r},\mathbf{r}';\beta)}{\partial\Omega^2}=0,\quad \frac{\partial W_N^{\Omega,\mathbf{x}_m}(\mathbf{r},\mathbf{r}';\beta)}{\partial\mathbf{x}_m}=0. \tag{37}$$

The perturbation series (35) is rapidly converging, in most cases already in the first-order approximation $W_1^{\Omega,\mathbf{x}_m}$ for the effective potential, and gives a reasonable estimate of the desired quantities.

III. COMPARISON OF THE PAIR POTENTIALS AND THEIR TEMPERATURE DEPENDENCE

We will now compare the accuracy of the pair potentials discussed above (or two-particle density matrices corresponding to these potentials), their temperature dependence, and range of applicability.

A. Full density matrix of electron-proton pair

In Fig. 2, we show the angular dependence of the full off-diagonal two-particle density matrix calculated with the off-diagonal Kelbg potential, ODKP (3), and its diagonal approximation, DKP (4). The density matrix is shown at several temperature values ($T=1\,000\,000$, 250 000, and 62 500 K) and several angular distances ($\phi=0,\pi/2,\pi$) between the vectors $\mathbf{r}\equiv\mathbf{r}_{ij}$, $\mathbf{r}'\equiv\mathbf{r}'_{ij}$ (in each of the figures, the top curves correspond to the case of parallel vectors, $\phi=0$, and the lowest curves to antiparallel vectors, $\phi=\pi$). Also, for reference, we give the off-diagonal density matrix obtained from the "exact" solution of the Bloch equation, cf. Sec. II C 1. At high temperatures, $T\geqslant 250\,000$ K, the Kelbg density matrix does not exhibit large deviations from the exact result. At $T=1\,000\,000$ K (left column of Fig. 2), the ODKP density matrix practically coincides with the exact solution, whereas the DKP approximation shows small deviations. In these cases, the perturbation expansion applies, $\Gamma\sim 0.15$. With decreasing temperature, the deviations from the exact results grow (see the middle column). To better understand the details of the deviations, we magnified the effect by including results for $T=62\,500$ K, which is far beyond the scope of the perturbation theory, $T\approx 0.4\ {\rm Ry}/k_B$, i.e., $\Gamma\approx 2.5$. Here we observe that, at the origin, the density matrix of the Kelbg potential is three times less than the exact one. The largest errors were found for the DKP, in particular, in the case when the vectors $\mathbf{r},\mathbf{r}'$ have the opposite direction ($\phi=\pi$).

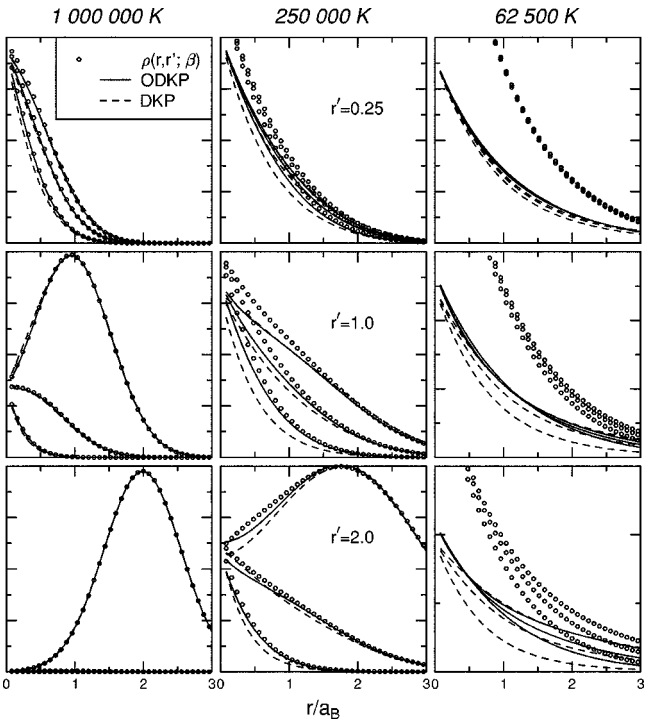

FIG. 2. The "exact" off-diagonal density matrix $\rho(\mathbf{r},\mathbf{r}';\phi)$ for an electron-proton pair vs the density matrix calculated with the diagonal (DKP) and off-diagonal (ODKP) Kelbg potentials. In all figures, results for three angular values are given as $\phi=0$ (upper curves), $\phi=\pi/2$ (middle), and $\phi=\pi$ (lower curves). The proton is located at the origin, and the vector $\mathbf{r}'$ (initial electron position) is fixed, $|\mathbf{r}'|=0.25$; 1.0; 2.0. The vector $\mathbf{r}$ (final electron position) is varied; ϕ is the angle between the vectors $\mathbf{r}$ and $\mathbf{r}'$.

The behavior of the full density matrix can be understood from the following considerations. The density matrix results from contributions of kinetic and potential energy operators, cf. Eq. (1). At small distances ($\mathbf{r}'=0.25$), the Coulomb at-

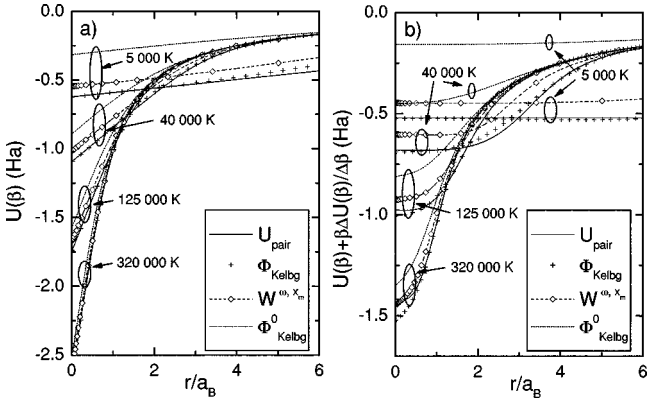

FIG. 3. (a) Diagonal effective electron-proton potential (in units of Ha) for several cases: the DKP $\Phi^0(\mathbf{r};\beta)$ (4), the improved DKP $\Phi(\mathbf{r};\beta)$ (8), variational potential $W_1^{\Omega,\mathbf{x}_m}$ (35), and pair potential U_p (27) corresponding to the "exact" density matrix. Each potential is given at three temperature values: 5000, 40 000, 125 000, and 320 000 K. (b) The function $U(\beta)+\beta\partial U(\beta)/\partial\beta$ for the same approximations and temperatures. The ovals include a set of curves corresponding to the denoted temperature.

traction between an electron and a proton dominates and, therefore, the density matrix shows an exponential decay. At the largest distance ($\mathbf{r}'=2.0$), kinetic and potential energy are of the same order and a Gaussian-like free-particle density matrix emerges, as can be clearly seen in the bottom left part of Fig. 2.

From this first comparison, we can conclude that both the DKP and the ODKP show satisfactory agreement with the exact result in the cases where perturbation theory applies, $T\gtrsim 2$ Ry. At lower temperatures, there is only qualitative agreement. The strongest deviations arise for small interparticle distances $\{\mathbf{r},\mathbf{r}'\}$, and this, as will be shown below, results from the incorrect height of the Kelbg potential at zero distance $\mathbf{r}=0$.

B. Effective interaction of electron-proton and electron-electron pairs

In Figs. 3(a) and 3(b), we show and compare the accuracy of several effective electron-proton potentials and their temperature derivatives obtained by various methods. As an "exact" reference potential to which the accuracy of other potentials is compared, we use $U_{\rm pair}$ obtained from the electron-proton pair density matrix calculated with the matrix squaring technique.

First, we note from Fig. 3(a) that, at given temperatures $T\leqslant 2$ Ry, the original Kelbg potential shows the largest deviations from the "exact" result, $U_{\rm pair}$. While the spatial derivative of the DKP coincides with that of $U_{\rm pair}$, a systematic offset of the DKP compared to $U_{\rm pair}$ is observed at the origin $\mathbf{r}=0$, which increases when the temperature is lowered. The agreement is satisfactory only for the curve corresponding to $T=320\,000$ K. The accuracy of the Kelbg potential becomes worse for quantities involving its temperature derivative. For example, for the total energy one has to compute the thermodynamic average of the function $\partial[\beta U(\beta)/\partial\beta]|_{U=\Phi^0_{\rm Kelbg}}$. This function is shown in Fig. 3(b). If multiplied by the Boltzmann factor $e^{-\beta U(\beta)}$, this function is a good estimate for the binding energy (E_b) of an electron-proton pair. In the case of a bound state, the main contribution to the energy comes from the region of small interparticle distance, $\mathbf{r}\lesssim 3a_B$. Therefore, the behavior of $\partial[\beta U(\beta)/\partial\beta]$ near the origin determines the accuracy of the calculations of the energy and other thermodynamic quantities. As we can see from the curve for 5000 K in Fig. 3(b), the depth of the DKP is much less than that of $U_{\rm pair}$ and, therefore, it gives too low a binding energy of $E_b\approx 0.16$ Ha, i.e., a factor of 3 too low compared with the true ground-state energy $E_b^0=0.5$ Ha.

As was already discussed in Sec. II B, the accuracy of the DKP can be improved with the additional fit parameter γ_{ij}. In Figs. 3(a) and 3(b), this potential is denoted as $\Phi_{\rm Kelbg}$. One can see that at all considered temperatures, $\Phi_{\rm Kelbg}$ practically coincides with $U_{\rm pair}$. Even in the case of strong coupling ($T=5000$ K), the agreement is very good.

The next potential shown in this figure is the variational potential, $W^{\omega,\mathbf{x}_m}$, introduced in Sec. II C 2. This potential is more accurate than the DKP and qualitatively reproduces the "exact" effective pair potential $U_{\rm pair}$ for temperatures $T=125\,000$ K, 320 000 K, and its derivative [see Fig. 3(b)]. The key point is that the *variational perturbation theory* [38] replaces the perturbation expansion in Γ (which does not converge for $\Gamma\gtrsim 1$) into another expansion, Eq. (34), which does not have this restriction. The results of this approach can be improved by taking into account higher-order terms in Eq. (34) (the results shown in the figure include only the first term, $n=1$). The convergence of Eq. (34) extends even to very strong coupling and has been successfully applied in field theory (39).

We mention that comparison with other effective potentials has been performed in our previous paper [1]. In particular, the "exact" pair potential was compared with the results of Barker [33] (the calculations of the pair potential by the direct eigenfunction summation) and the Deutsch potential. Good agreement has been found with the data of Barker [33], while the deviations of the Deutsch potential turned out to be slightly larger than that of the Kelbg potential. The reason for this difference is that the Deutsch potential has an incorrect spatial derivative, $U'_{\mathbf{r}}$, for $\mathbf{r}\lesssim 3a_B$.

Next, in Fig. 4, we compare pair distribution functions (PDF) of two electrons in singlet and triplet states for different temperatures, obtained from the expression with the effective potential,

$$g(\mathbf{r})\propto e^{-\beta U^{S(T)}(\mathbf{r})}. \tag{38}$$

Due to the Pauli principle in Fig. 4(a), the PDF goes to zero as $\mathbf{r}_{ee}\to 0$. On the other hand, for electrons in a singlet state [Fig. 4(b)], this happens only if the temperature is decreased to 31 250 K, where the potential energy dominates the kinetic energy. The three lines in Fig. 4(a) show three cases: (i) and (ii) when as an effective potential in Eq. (15) we substitute the "exact" pair potential and the Kelbg potential; (iii) when in Eq. (17) we substitute the Kelbg potential. In the last case, the exchange contribution from the potential function is neglected. This, as shown in Fig. 4(a), becomes important only for the temperature 31 250 K and below. Similarly, in

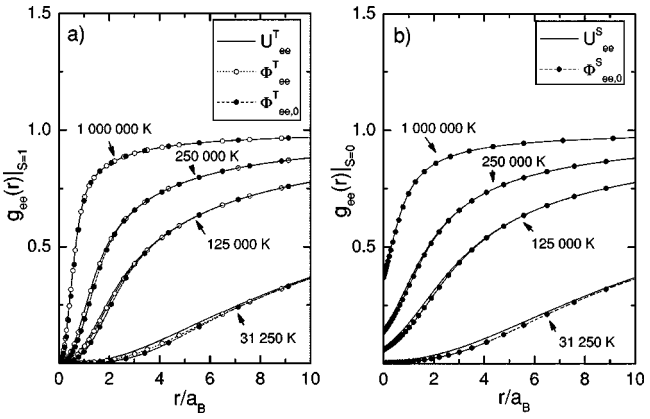

FIG. 4. Pair distribution function for a pair of electrons. (a) In a triplet state (parallel spins, $S=1$). Cases compared are Eq. (14), using for U_{ee} the "exact" pair potential, $g \propto e^{-\beta U^T_{ee}}$, the Kelbg potential, $g \propto e^{-\beta \Phi^T_{ee}}$, and Eq. (17) with the Kelbg potential, $g \propto e^{-\beta \Phi^T_{ee,0}}$. (b) In a singlet state (antiparallel spins, $S=0$), Eq. (14) with the "exact" pair potential, $g \propto e^{-\beta U^S_{ee}}$, and Eq. (17) with the Kelbg potential, $g \propto e^{-\beta \Phi^S_{ee,0}}$. The pair distribution functions are shown for temperatures, $T=31\,250$, 125 000, 250 000, and 1 000 000 K.

Fig. 4(b) we compare two curves [cases (i) and (iii) of Fig. 4(a)] corresponding to the "exact" pair potential and the Kelbg potential.

One can note that the overall accuracy of the Kelbg potential for description of two particles with the same charge (even without improving its value at the origin with γ) is significantly better (compared to the results with the "exact" pair potential) than for particles with opposite charge, cf. Fig. 3. This is due to the absence, in this case, of contributions from bound states.

In Sec. V, these pair correlation functions will be compared with those for a hydrogen plasma obtained by molecular-dynamics simulations, see Fig. 9.

In the next section, we discuss application of quantum pair potentials in thermodynamic calculations using Feynman trajectories in imaginary time (PIMC).

IV. QUANTUM PAIR POTENTIALS IN THE PATH INTEGRAL MONTE CARLO METHOD

It is well known (see, for example, the discussion in Chap. 12 of [38]) that the singularity of the attractive Coulomb potential causes difficulties in the Euclidian path integral. The energy of the path can be lowered indefinitely by an almost stretched configuration (a path is presented as a straight line along an imaginary time axis) which corresponds to a slowly moving particle sliding down to the $-e^2/\mathbf{r}$ abyss. This phenomenon is called *path collapse.*

One possibility to prevent this effect is to use a modified "regularized" Coulomb potential which has a cutoff at $\mathbf{r}=0$. This procedure, however, is quite arbitrary, and the results are sensitive to the chosen cutoff parameters. Of course, in nature, these difficulties are prevented by quantum fluctuations which equip the path with a configurational entropy. The latter must be sufficiently singular to produce a regular free energy bounded from below. The inclusion of quantum fluctuations in the Euclidean action of the Feynman path pieces smoothes the singular Coulomb potential, producing an effective potential that is finite at the origin, and *path collapse* is avoided. This again shows the importance of effective potentials, specifically, in "quasiclassical" simulations (classical Monte Carlo and molecular-dynamics methods). Of great importance are potentials which have a closed analytical form. In this case, for many thermodynamic quantities it is possible to obtain analytical solutions.

For simulations of correlated quantum many-body systems which are based on *first principles,* the initial many-body Hamiltonian with the true singular Coulomb energy operator is considered and solved to find some effective many-body interaction potential. For this approach, it is important that in the high-temperature limit the N-particle density matrix can be expanded in terms of two-particle, three-particle, etc., contributions. If the temperature is sufficiently high, then all contributions except the first one, which takes into account two-particle correlations, can be omitted. As a result, the following approximation for the N-particle density matrix holds:

$$\rho(\mathbf{R},\mathbf{R}';\tau) \approx \prod_i^N \rho^{[1]}(\mathbf{r}_i,\mathbf{r}'_i;\tau) \prod_{j<k} \frac{\rho^{[2]}(\mathbf{r}_j,\mathbf{r}_k,\mathbf{r}'_j,\mathbf{r}'_k;\tau)}{\rho^{[1]}(\mathbf{r}_i,\mathbf{r}'_i;\tau)\rho^{[1]}(\mathbf{r}_k,\mathbf{r}'_k;\tau)} + O(\rho^{[3]}), \tag{39}$$

where $\mathbf{R}=\{\mathbf{r}_1,\ldots,\mathbf{r}_N\}$ specifies coordinates of all N particles, and $\rho^{[1]}(\rho^{[2]})$ is the single- (two-) particle density matrix. The above *pair* approximation is usually used in PIMC simulations [37]. The N-particle density matrix $\rho(\beta)$ contains complete information about the system with the observables given by

$$\langle \hat{O} \rangle = \frac{\mathrm{Tr}[\hat{O}\,\hat{\rho}(\beta)]}{\mathrm{Tr}[\hat{\rho}(\beta)]} = \frac{\int d\mathbf{R} \langle \mathbf{R}|\hat{O}\,\hat{\rho}(\beta)|\mathbf{R}\rangle}{\int d\mathbf{R} \langle \mathbf{R}|\hat{\rho}(\beta)|\mathbf{R}\rangle}. \tag{40}$$

Due to the exponential form, the N-particle density operator $\hat{\rho}(\beta)=e^{-\beta\hat{H}}$ can be factorized (in analogy to the matrix squaring method above) as $\hat{\rho}(\beta)=[\hat{\rho}(\tau)]^M$ with $M=\beta/\tau$. Consequently, the N-particle density operator $\hat{\rho}(\beta)$ is expressed in terms of density operators at an M times higher temperature $1/\tau=Mk_BT$. If M is chosen sufficiently large, then one can apply the pair approximation (39). Thus, accurate results for the quantum pair potentials and, consequently, the pair density matrix will allow the calculation of the density matrix of the whole N-particle system. Here we are not interested in the investigation of the accuracy of the approximation given in Eq. (39) but concentrate on the two-body problem where Eq. (39) is exact.

It is clear that the observables (40) computed with the approximate pair-density matrix $\rho^{[2]}$ contain an error of the order $O(1/M^2)$. Below, we will investigate the convergence, as a function of M, of the main thermodynamic properties (total energy and e-p pair distribution) for an electron-proton

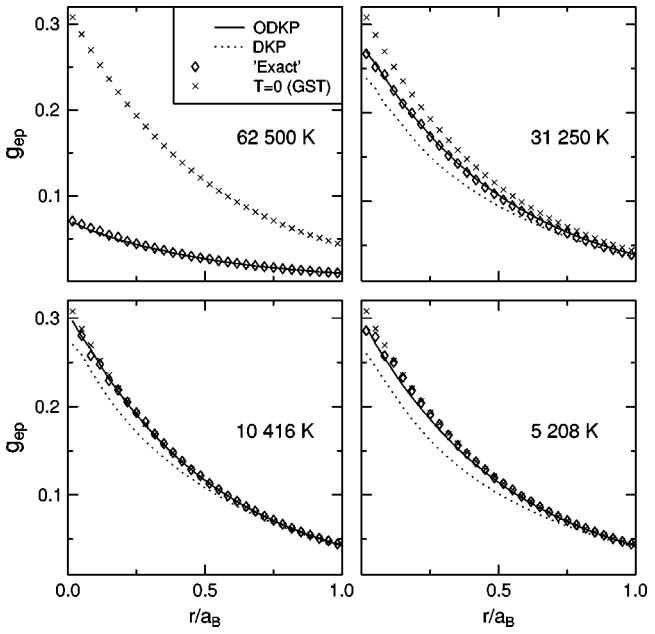

FIG. 5. Proton-electron pair correlation functions, $g_{ep}(\mathbf{r})$, from PIMC simulations with the "exact" pair density matrix (diamonds), the DKP (dots), and the ODKP (full line). Temperature values are as indicated in the figure parts: $T=5\,208$, 10 416, 31 250, and 62 500 K. For comparison, $T=0$ "GST" denotes the pair correlation function (shown by crosses) corresponding to the ground state of a hydrogen atom.

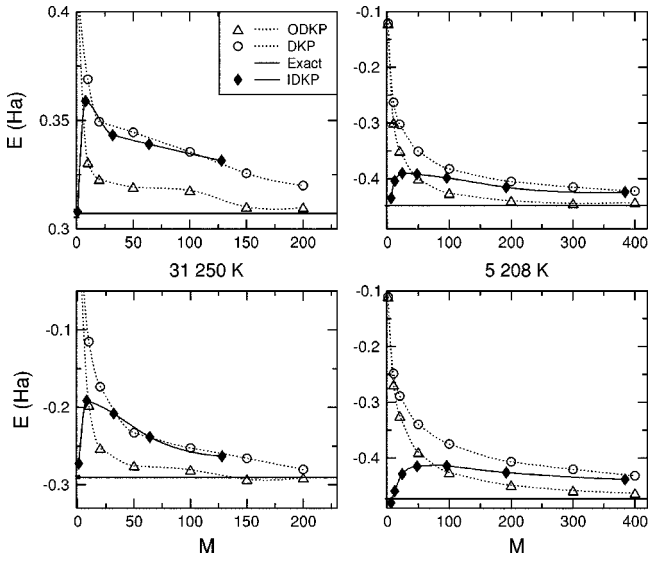

FIG. 6. PIMC results for the internal energy of the proton-electron pair using "exact" pair density matrix, DKP, ODKP, and Improved Kelbg potential (IDKP) vs different number of factorization factors M.

pair using for the pair density matrix $\rho^{[2]}$ results computed with the off-diagonal and the diagonal Kelbg potential.

Comparison of the diagonal and the off-diagonal Kelbg potential in the example of a hydrogen atom

We consider a hydrogen atom in a box with periodic boundary conditions (box size $L=20\,a_B$) at several temperatures, $T=31\,250-62\,500$ K, when the hydrogen atom can ionize into free particles, as well as for the case $T<10\,000$ K, when there is essentially only the contribution from the atomic ground state. First, in Fig. 5 we show the *e-p* pair distribution functions (normalized to the volume $dV=4\pi\mathbf{r}^2d\mathbf{r}$).

For temperatures $T=5208$ K and 10 416 K, the hydrogen atom does not decay into free particles during the duration of a typical simulation run ($\sim 10^6$ Monte Carlo steps). In the figures, the "exact" pair correlation function is compared with the one obtained with the off-diagonal and diagonal Kelbg potentials, respectively (the number of factorization factors for the density matrix was chosen to be $M=400$). We found that the best accuracy is achieved for the off-diagonal Kelbg potential and $M\gtrsim 200$; in this case the ODKP pair correlation function practically coincides with the exact result ($T=0$ "GST" curve in the two upper panels of Fig. 5).

At elevated temperatures, $T=31\,250$ K and 62 500 K, ionization of the hydrogen atom occurs, but due to the periodic boundary conditions, the free particles cannot go to infinity but, when reaching the boundary, are returned back in the simulation box and have a finite probability for a formation of a bound state again. Thus, this simulation captures the region of partial ionization. As the temperature is increased, the ionization probability also increases, leading to a significant drop in the height of the proton-electron pair distribution function at the origin compared to the ground-state probability function $\Psi_0^2(\mathbf{r})$ (see Fig. 5, plots for $T=31\,250$ K and $T=62\,500$ K).

In Fig. 6, we analyze the convergence of the internal energy in PIMC simulations with a varying number of high-temperature factors M. In particular, we compare independent simulations with the diagonal and off-diagonal Kelbg density matrices, respectively. The "exact" energy value for the considered temperatures is given by the solid line and is obtained from PIMC simulations using the "exact" pair density matrix, cf. Sec. II C 1. The internal energy was obtained using the thermodynamic estimator, $\langle E\rangle=-(\partial/\partial\beta)\ln Z$, where Z is the partition function. Comparing the *diagonal* and *off-diagonal* cases, one can note that the ODKP density matrix shows much better and faster convergence to the exact energy value. The improved diagonal Kelbg potential gives the exact result only for the diagonal density matrix (the special case when $M=0$, and the density matrix is not factorized). For any finite number of factors, $M\geqslant 1$, one makes an error in Eq. (2) by substituting the off-diagonal potential with its diagonal approximation. This error decreases with the increase of temperature (or, equivalently, with the number of factors M) because, as the temperature increases, the particle extension (given by the deBroglie wavelength) is reduced, and the difference in the potential at points $\mathbf{r}$ and $\mathbf{r}'$ vanishes. This explains why the improved Kelbg potential for a small number of factors $1\leqslant M\leqslant M_{\rm cr}$ shows an increasing deviation and for $M>M_{\rm cr}$ converges toward the "exact" result. The value of $M_{\rm cr}$ (largest deviation) is in the range of $1\cdots 100$, where the small (large) number corresponds to high (low) temperature, cf. Fig. 6.

A simple estimate shows that the relative error of the total energy, in the diagonal approximation, depends on factoriza-

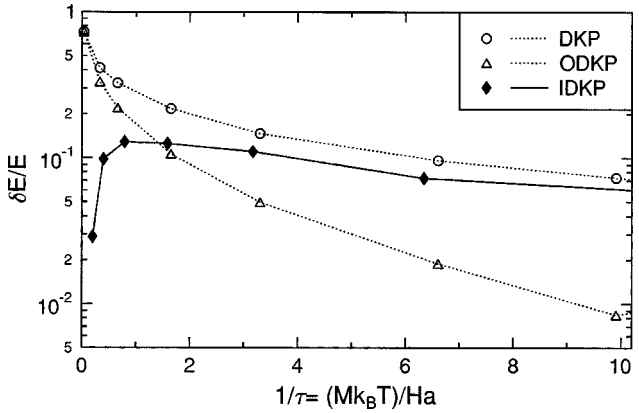

FIG. 7. Relative error in the internal energy of the proton-electron pair from PIMC simulations with the diagonal, off-diagonal and improved Kelbg potential (IDKP) vs temperature argument in the two-particle density matrix $1/\tau$.

tion number M as $\delta E/E \approx \gamma\tau^2$, $\tau=\beta/M$. In contrast, using the off-diagonal potential, the error converges much faster, $\delta E/E \approx \gamma\tau^3$. This fact is illustrated in Fig. 7, where the logarithm of the relative error, $\log(\delta E/E)$, is shown as a function of the inverse of the temperature used in the high-temperature factors, $1/\tau$. In this figure, we compare the behavior of the error for the same set of temperatures as in Fig. 6. In Fig. 6, we also add simulation results using the *improved diagonal* Kelbg potential (solid line). Its accuracy is better than that of the ODKP at low temperatures (small values of M), but at high temperatures both are comparable.

The main conclusion that can be drawn from the presented PIMC results is that, at an equal number of factorization factors M, simulations with the off-diagonal Kelbg potential are significantly more accurate in reproducing the "exact" thermodynamic results of a hydrogen atom. Besides, the full off-diagonal density matrix contains valuable information about the spatial electron distribution around the proton, which is lost in the end-point approximation. Further, we expect that the best results will be obtained using *an improved off-diagonal* Kelbg potential, which has the correct zero-point value and contains the complete angular dependence of the pair density matrix which, however, is beyond the scope of the present paper.

V. MOLECULAR-DYNAMICS SIMULATIONS

In this section, we apply the improved Kelbg potentials in classical molecular-dynamics simulations of dense hydrogen. Classical MD simulations of dense plasmas have been performed by many authors before, where the classical collapse of an electron into a proton is usually avoided by some cutoff or "regularization" of the Coulomb potential at small distances. By using the effective quantum pair potentials obtained from the exact solutions of the Bloch equations, we expect to have the correct pair interactions at short distances. This should not only prevent any collapse, but also correctly reproduce the formation of hydrogen atoms and thus allow us to obtain improved MD simulation results. However, since these potentials are derived from pure equilibrium considerations, there is no ad hoc proof that they will necessarily be accurate for the description of dynamical behavior as well (in particular under strong nonequilibrium conditions). We, therefore, concentrate in the present analysis on correlated partially ionized hydrogen in *thermodynamic equilibrium.* The results obtained below confirm that, indeed (at least in equilibrium), the quantum pair potentials are well suited for use in the interparticle force terms in classical MD.

Classical MD simulations incorporate all interparticle collision processes and are thus not restricted with respect to the coupling parameter Γ in a classical system. With the use of effective quantum pair potentials, we expect, in addition, to capture dominant features of the quantum nature of microparticles, such as quantum diffraction and spin effects. Thus, these simulations could be called "semiclassical" MD. Having access not only to improved electron-ion potentials but also to spin-dependent electron-electron potentials allows us to consider also spin effects by simulating electrons with different spin projections as two independent particle species. While in this paper no spin-flip processes are considered [40], our model is capable of treating spin as an additional degree of freedom. In particular, it should allow us to describe spin polarization, spin interaction with magnetic fields, spin density waves, and so on. In this paper, we focus on static properties, such as internal energy, and radial distribution functions. Investigation of dynamical properties and of spin density fluctuation is the aim of a forthcoming paper.

We consider a dense, degenerate hydrogen plasma at two densities corresponding to the Brueckner parameter $\mathbf{r}_s = \bar{\mathbf{r}}/a_B = 4$ and $\mathbf{r}_s = 6$ and temperatures $T = 31\,250$, 50 000, 62 500, 125 000, and 166 670 K. These parameter values correspond, respectively, to $\Gamma = 2.53$, 1.58, 1.26, 0.63, and 0.47 for $\mathbf{r}_s = 4$; and $\Gamma = 1.68$, 1.05, 0.84, 0.42, and 0.32 for $\mathbf{r}_s = 6$.

The simulation box of our system, with the length $L = [n/(N_p + N_e^{\uparrow} + N_e^{\downarrow})]^{1/3}$, contains $N_p = 200$ protons, $N_e^{\uparrow} = 100$ electrons with spin up and an equal number of electrons, and $N_e^{\downarrow} = 100$ with spin down. We keep the condition of the electroneutrality by taking $N_p = N_e^{\downarrow} + N_e^{\uparrow}$. Details of the numerical algorithm can be found in Ref. [22].

Since MD, in contrast to PIMC, involves only diagonal interaction potentials, we choose the following expressions: for the interaction between electrons and protons, protons and protons, and electrons with opposite spin, we use the improved Kelbg potential, Eq. (8), with the fit parameters given by Eqs. (22) and (23), respectively. The interaction between electrons with the same spin projection is described by the diagonal antisymmetric potential, Eq. (17). Further, to properly account for the long-range character of the potentials, we used the standard Ewald procedure as outlined in Ref. [22]. However, in contrast to the rather involved expressions of Ref. [22] for a one-component plasma, here we restrict the potential energy sum to the proper sum only in *real space* (due to an additional partial screening of the interaction between particles of the same charge by particles of opposite charge). We do not reproduce these lengthy expressions here, but mention that the value of the parameter α defined in Ref. [22] was chosen to be $\alpha = 5.6/L$, and we take Five vectors in every direction in *the reciprocal space.* This gives some computational-cost advantage in the computation of the forces compared to Ref. [22].

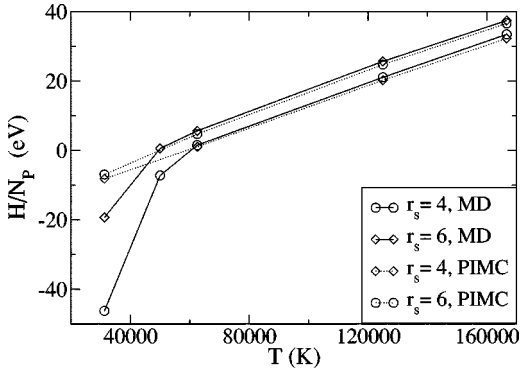

FIG. 8. Semiclassical MD results (full lines) for the internal energy per hydrogen atom at densities $\mathbf{r}_s=4,6$ vs temperature. The results of restricted PIMC simulations by Militzer [41] are shown for comparison (dashed lines). Symbols indicate the five temperatures for which MD simulations have been performed: $T=31\,250$, 50 000, 62 500, 125 000, and 166 670 K (solid lines). The pair approximation breaks down around 50 000 K at the molecule binding energy.

In Fig. 8, we plot the internal energy per atom as a function of temperature for two densities and compare it to the path integral Monte Carlo results of Militzer [41]. One can note that for high temperatures, the energies of MD and PIMC simulations coincide very well and lie within the limits of statistical errors. This is an important test for the simulation, and this agreement was expected due to the asymptotic character of the Kelbg potential as a rigorous weak-coupling result. Moreover, we observe good agreement between MD and PIMC results at temperature as low as approximately 50 000 K, corresponding to a coupling parameter $\Gamma=3$. This is a remarkable extension of "semiclassical" molecular dynamics into the regime of moderate coupling and moderate degeneracy.

Below a critical temperature of about 50 000 K, deviations from the PIMC results start to grow rapidly; the MD results for the energy are lower than the PIMC results. It is very interesting to analyze the reasons for these deviations, as this may suggest directions for further improvements. These deviations are not due to a failure of the quantum pair potentials. The quantum pair potentials remain exact in the whole temperature range. In contrast, the observed deviations of the MD results from the PIMC data arise as a consequence of many-particle effects, i.e., correlations. This explanation is confirmed by a detailed inspection of the microscopic particle configurations in the simulation box. At high temperatures, the particle trajectories are those of a fully ionized classical plasma. At temperatures below 1 Ry, we observe an increasing number of electrons undergoing strong deflections on protons and eventually performing quasibound trajectories. Most of these electrons remain "bound" only for a few classical orbits and then leave the proton again. Averaged over a long time, our simulations are able to reveal the degree of ionization of the plasma. At the same time, we observe occasional events when three or more particles are close to each other for the duration of one or more orbits, reflecting the appearance of hydrogen molecules H_2, molecular ions H_2^+, etc.

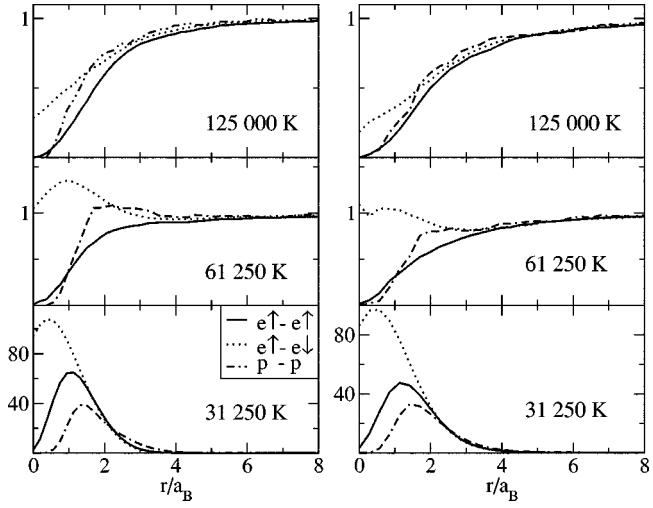

FIG. 9. Electron-electron and proton-proton radial pair distribution functions for a correlated hydrogen plasma with $\mathbf{r}_s=4$ (left row) and $\mathbf{r}_s=6$ (right row) for $T=125\,000$, 61 250, and 31 250 K (from top to bottom).

If the temperature is lowered below approximately $T=50\,000$ K, we observe a strong increase in molecule formation and even an aggregation of many molecules into clusters with an interparticle distance close to $1a_B$. This turns out to be the reason for the observed very low energy because the attractive Coulomb interaction contributions are becoming dominant in the total energy. Of course, this behavior is not surprising: while all pair interaction processes are modeled correctly even at low temperature (which is assured by the fit parameters in the improved Kelbg potentials), as soon as three or more particles are close together, three-particle and higher-order correlations are strong (they, in particular, account for the formation of the larger bound-state complexes described above). However, in the derivation of the quantum potentials, it was assumed that three-particle and higher correlations could be neglected that formed the basis for the use of pair potentials in modeling the whole N-particle system. While molecular dynamics, of course, includes any level of correlations, the use of the present potentials means that *quantum corrections to three-body (and higher-order) interactions* are not adequately captured. Therefore, it is no surprise that this approximation breaks down at sufficiently low temperature, and that this breakdown occurs around the temperature corresponding to the binding energy of hydrogen molecules. From this we can conclude that molecule formation sets the limit of the applicability of the present semiclassical MD simulations.

Let us now turn to a more detailed analysis of the spatial configuration of the particles in the MD simulations.

In Fig. 9, the radial pair distributions between all particle species with the same charge are plotted at two densities. Consider first the case of $T=125\,000$ K (upper panel). For both densities, all functions look qualitatively the same, showing a depletion at zero distance due to Coulomb repulsion. Besides, there are differences which arise from the spin properties. Electrons with the same spin show a slightly broader "Coulomb hole" around $\mathbf{r}=0$ than the protons, be-

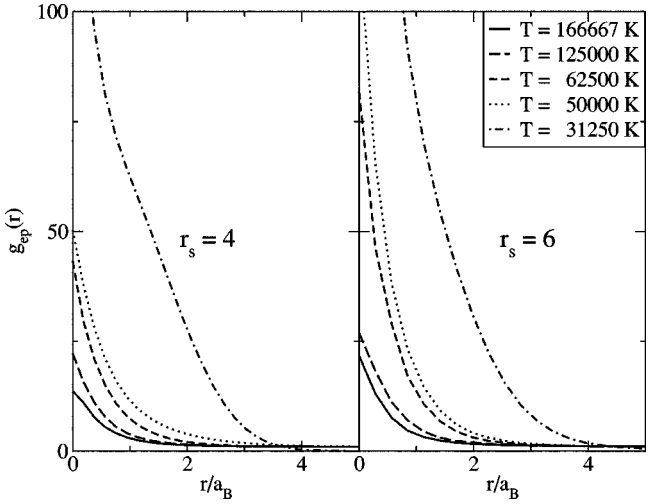

FIG. 10. Electron-proton radial pair distribution functions at $\mathbf{r}_s=4$ (left figure) and $\mathbf{r}_s=6$ (right figure) and five temperatures: $T=166\,667$, 125 000, 62 500, 50 000, and 31 250 K.

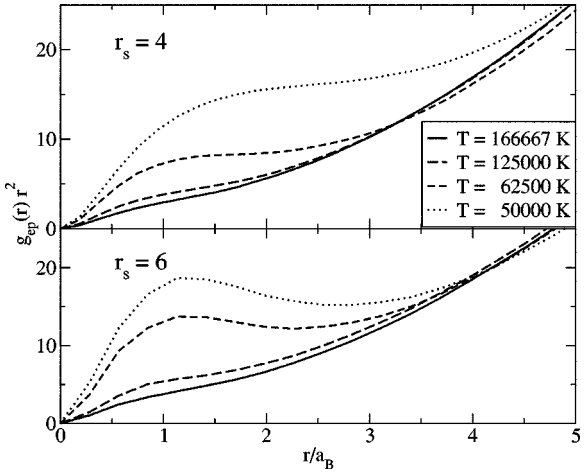

FIG. 11. Electron-proton radial pair distribution functions multiplied by $\mathbf{r}^2$. Same data as in Fig. 10.

cause the Pauli principle yields an additional repulsion of the electrons (this effect is much weaker for two protons due to their much smaller deBroglie wavelength). This trend is reversed at lower temperature (see middle panel), which is due to the formation of hydrogen atoms; see also Fig. 11 below. In this case, the electron trajectories are "spread out" around the protons, giving rise to an increased probability of close encounters of two electrons in different atoms compared to two protons.

Now, let us compare electrons with parallel versus antiparallel spins. In all cases, we observe a significantly increased probability to find two electrons with opposite spin at small distances below one Bohr radius, which is due to the missing Pauli repulsion in this case. This trend increases as the temperature is lowered because of quantum effects and thus convincingly confirms that spin effects are correctly reproduced in our MD simulations.

It is interesting to compare the electron PDF's of Fig. 9 with the results of the QMC calculation, see, e.g., the curves for 125 000 K in Fig. 4. The general trend is that, at small distances, corresponding to $\mathbf{r}\lesssim 4a_B$, the MD curves are significantly higher than the QMC results. The reason for this increase of the probability to find two electrons at small distances is easy to understand: the QMC results correspond to an isolated pair of electrons. In contrast, the MD simulations yield the two-electron correlation in the presence of the surrounding plasma particles. These plasma particles partially screen the *e-e* repulsion. This effect is reduced when the density is lowered from $\mathbf{r}_s=4$ to $\mathbf{r}_s=6$ (Fig. 9). In the limit of zero density, the PDF is given by the QMC result.

Before analyzing the lowest temperature in Fig. 9, let us consider the electron-proton pair distributions which are shown in Fig. 10. As the temperature is lowered, we observe a strong increase in the probability of finding an electron close to a proton. In contrast to the classical case of a collapse (see above), here the probability is finite. Multiplying these functions by $\mathbf{r}^2$ gives essentially the radial probability, which is plotted in Fig. 11. Here, lowering the temperature leads to the formation of a shoulder at around $1.5a_B$, which is due to the formation of hydrogen atoms. This conclusion is confirmed by inspection of the corresponding quasibound electron trajectories, as discussed above. At the lowest temperature ($T=50\,000$ K) shown in Fig. 11, the observed most probable electron distance is not $1a_B$, as in the case of the hydrogen ground state, but is larger as a consequence of the considerable kinetic energy of the particles. We expect that at even lower temperatures, the most probable radius would tend towards $1a_B$, but this temperature range is not realistically modeled due to molecule and cluster formation.

While the description of correlated complexes of more than two particles is certainly beyond the present pair approximation model, several features of partially ionized and partially dissociated hydrogen plasmas are reproduced correctly. At 62 500 K and $\mathbf{r}_s=6$ (right center part of Fig. 9), the simulations show the first weak signature of molecule formation—see the maximum of the *p-p* pair distribution function around $\mathbf{r}=2a_B$ and the maximum of the pair distribution function of electrons with antiparallel spins around $\mathbf{r}=1.5a_B$. Further lowering of the temperature by a factor of 2 (lower panel of Fig. 9) confirms this trend: the *p-p* functions exhibit a clear peak very close to $\mathbf{r}=1.4a_B$—the theoretical *p-p* separation in H_2 molecules. At the same time, the *e-e* functions have a clear peak around $\mathbf{r}=0.5a_B$, in the case of opposite spins, and $\mathbf{r}=1.2a_B$, for parallel spin projections. The first case comes rather close to the true quantum-mechanical H-H bound state (singlet) with the electron wave function predominantly concentrated between the two protons. On the other hand, this electron peak should extend to the right of the *p-p* peak, and no such pronounced peak is expected for electrons with the same spin.

We conclude that even the formation and spatial dimension of hydrogen molecules appear to be captured surprisingly well in these simulations. The main difficulty appears to arise not on the level of four-particle correlations but on the level of six-particle correlations: in the simulations, nothing prevents two "bound" atoms from binding to a third and more atoms. The overall attractive Coulomb interaction makes it, below 50 000 K, energetically favorable to form

large clusters consisting of more than two atoms, explaining the strong decrease of the internal energy at $T=31\,250$ K, cf. Fig. 8. In reality, complexes of two molecules do exist, but they have a very low binding energy which is due to subtle compensation effects arising from repulsive exchange interaction between the electrons which go far beyond the level of pair interactions [42].

VI. USE OF THE QUANTUM PAIR POTENTIALS IN DENSITY-FUNCTIONAL THEORY

The effective quantum potentials have been introduced to represent the equilibrium two-particle density matrix and subsequently generalized to incorporate many-body Coulomb coupling effects. There are other many-body coupling effects due to degeneracy or exchange correlations. For some applications, it may be useful to incorporate these directly in the effective pair potentials to extend their validity to still lower temperatures, as was demonstrated in the example of classical MD above.

In this section, we describe the usefulness of the effective quantum potentials for a completely different theoretical approach, namely density-functional theory (DFT). In doing so, the role of effective quantum potentials with degeneracy effects is illustrated as well.

DFT is a formal structure in which nonperturbative approximations can be introduced to describe strong-coupling effects [43]. Although there are both classical and quantum versions of DFT, the classical form does not apply to a system of electrons and positive ions due to Coulomb divergence. One possibility is to postulate classical statistical mechanics using the effective quantum potentials described above, which allows the removal of the singularity. Alternatively, the proper quantum formulation can be used from the outset and the effective quantum potentials "derived" as a tool in the process of computing properties of interest [44]. This second approach will be used here.

In essence, DFT is a variational means to derive an equation for the charge density induced by an external potential. If that potential is taken to be the same as the potential of one of the charges in the system, the resulting density is in fact formally identical to the equilibrium pair correlation function, or diagonal element of the two-particle density matrix. The density obeys a known nonlinear integral equation—a generalization of the Boltzmann-Poisson equation. However, in practice, the direct solution of this equation is seldom attempted. Instead, an equivalent set of self-consistent one-particle Schrödinger equations, the Kohn-Sham equations [45], are solved to construct the charge density. Yet it might be very useful to recall the existence of an alternative direct approach which becomes practical if an appropriate quantum pair potential is introduced. This is illustrated in more detail as follows.

Consider a quantum system in the presence of external sources that can be described by an additive potential,

$$\hat{V}=\sum_{\alpha}\sum_{i=1}^{N_\alpha}\hat{V}_\alpha(\mathbf{q}_{i\alpha}). \tag{41}$$

Here α denotes a species and $\mathbf{q}_{i\alpha}$ is the position operator of particle i of species α. The caret on the potentials is used to distinguish the quantum operator from its corresponding function. In general, each species may have a different form for the coupling to the external sources. The potential also can be written in terms of the density operators for each species,

$$\hat{V}=\int d\mathbf{r}\sum_{\alpha}V_\alpha(\mathbf{r})\hat{n}_\alpha(\mathbf{r}),\quad \hat{n}_\alpha(\mathbf{r})=\sum_{i=1}^{N_\alpha}\delta(\mathbf{r}-\mathbf{q}_{i\alpha}). \tag{42}$$

The details of the remainder of the Hamiltonian are not important at this point. For this many-body system with external sources, the theorems of density-functional theory apply in the following form. First, a functional of the average densities, $\hat{n}_\alpha(\mathbf{r})$, averaged over an equilibrium grand-canonical ensemble is constructed (the generalization to other equilibrium ensembles has been carried out). This is done in two steps. First, the equilibrium grand potential for the system is considered formally,

$$\beta\Omega_e=-\ln\sum_{\{n_\alpha\}}\mathrm{Tr}\,e^{-\beta(H-\sum_\alpha\mu_\alpha n_\alpha)}. \tag{43}$$

The density for the various species is obtained (formally) by functional differentiation with respect to the potentials,

$$\Omega_e=\Omega_e(\{\mu_\alpha-V_\alpha\}),\quad n_{e\alpha}(\mathbf{r})=-\frac{\delta\Omega_e}{\delta[\mu_\alpha-V_\alpha(\mathbf{r})]}. \tag{44}$$

The density equation is inverted (formally) to get the external potentials as functionals of the average densities,

$$V_\alpha=\mathcal{V}_\alpha(\mathbf{r}|\{n_{e\sigma}\}), \tag{45}$$

and a Legendre transformation is performed to construct the free energy as a functional of the densities rather than the chemical potentials,

$$F(\{n_{e\alpha}\})=\Omega_e(\{\mu_\alpha-\mathcal{V}_\alpha\})+\sum_\alpha\int d\mathbf{r}[\mu_\alpha-\mathcal{V}_\alpha(\mathbf{r}|\{n_{e\sigma}\})]n_{e\alpha}(\mathbf{r}). \tag{46}$$

The crucial second step is to extend this functional to *arbitrary density fields*,

$$F(\{n_{e\alpha}\})\rightarrow F(\{n\}). \tag{47}$$

The main task of density-functional theory is now to construct the density functional

$$\Omega_V(\{n\})\equiv F(\{n\})-\int d\mathbf{r}[\mu_\alpha-V_\alpha(\mathbf{r})]n_\alpha(\mathbf{r}), \tag{48}$$

where, in this definition, $V_\alpha(\mathbf{r})$ is *not* considered to be a functional of the density. The main theorem of density-functional theory is then that this functional has an extremum at the equilibrium density,

$$\frac{\delta\Omega_V(\{n\})}{\delta n}=0=\frac{\delta F(\{n\})}{\delta n}-[\mu_\alpha-V_\alpha(\mathbf{r})],$$

$$\Rightarrow n=n_{e\alpha}. \tag{49}$$

Furthermore, the value of the functional at the equilibrium density is clearly the equilibrium grand potential

$$\Omega_V(\{n\}) = \Omega(\{\mu_\alpha - \mathcal{V}_\alpha\}).$$

In practice, an approximate free-energy functional $F(\{n\})$ is written and Eq. (49) is solved to obtain the equilibrium density. This density is then used to evaluate the equilibrium grand potential and determine all equilibrium thermodynamic properties. Structural properties can be obtained as well by choosing the external potential to be the same as that for interaction among the system particles. In other words, the source is chosen to be a particle of the same type as those comprising the many-body system. The densities $n_{e\alpha}$ become equilibrium pair correlation functions.

How should the functional $F(\{n\})$ be constructed? There is clearly a part associated with an ideal gas, and an energy due to the direct Coulomb interactions. These can be identified explicitly. In addition, there are the more difficult parts due to exchange and correlations. Consequently, it has become standard practice to write the free energy as

$$F[n] = F^{(0)}(\{n\}) + \frac{1}{2}\sum_{\alpha,\sigma}\int d\mathbf{r}d\mathbf{r}' V_{\alpha\sigma}(\mathbf{r}-\mathbf{r}')n_\alpha(\mathbf{r})n_\sigma(\mathbf{r}') + F_{\rm xc}(\{n\}), \tag{50}$$

where $F^{(0)}(\{n\})$ is the free energy for the noninteracting system, the second term is the contribution from the direct Coulomb interaction, and $F_{\rm xc}(\{n\})$ denotes the remaining contributions due to interactions from exchange and correlations. Then the extremum condition (49) becomes [44]

$$\mathcal{V}_\alpha^{(0)}(\mathbf{r}|\{n_\sigma\}) = V_\alpha(\mathbf{r}) + \sum_\sigma \int d\mathbf{r}d\mathbf{r}' V_{\alpha\sigma}(\mathbf{r}-\mathbf{r}')n_\sigma(\mathbf{r}') + \frac{\delta F_{\rm xc}(\{n\})}{\delta n_\alpha(\mathbf{r})}, \tag{51}$$

with $\mathcal{V}_\alpha^{(0)}(\mathbf{r}|n)$ denoting the functional (45) for an ideal gas. Determination of this functional is the central issue of the discussion here, and we will show that it is closely related to the Kelbg potential analyzed in the bulk of this paper.

The definition of the functional $\mathcal{V}_\alpha^{(0)}(\mathbf{r}|n)$ is straightforward from the representation of the density for an *ideal Fermi gas* in the external potentials,

$$n_\alpha(\mathbf{r}) = \langle\mathbf{r}|(e^{\beta[(p^2/2m_\alpha)+\hat{V}_\alpha-\mu_\alpha]}+1)^{-1}|\mathbf{r}\rangle. \tag{52}$$

This is a single-particle problem. The right side is clearly a functional of V_α through the dependence of the eigenvalues of $(p^2/2m_\alpha)+\hat{V}_\alpha$ on the form of the external potential. Interestingly, even at the level of an ideal gas, determination of this functional is nontrivial. In the *nondegenerate limit,* this equation for the density becomes

$$n_\alpha(\mathbf{r}) \to \langle\mathbf{r}|e^{-\beta[(p^2/2m_\alpha)+\hat{V}_\alpha-\mu_\alpha]}|\mathbf{r}\rangle. \tag{53}$$

If the external potential is chosen to be a Coulomb source, then Eq. (53) becomes equivalent to the diagonal elements of the two-particle density matrix in relative coordinates, which has exactly the form of the pair distribution function used to define the effective quantum pair potential, cf. Eq. (27).

Once the exchange and correlation free-energy functional is specified (guessed), Eq. (51) provides a set of closed *classical* integral equations for the equilibrium densities. As will be seen below, a leading approximation is the usual Boltzmann-Poisson representation in terms of semiclassical potentials. The primary technical difficulty in this prescription is the determination of $\mathcal{V}_\alpha^{(0)}(\mathbf{r}|n)$. Kohn and Sham noted that Eq. (51) defines an effective single-particle potential and therefore is formally equivalent to an ideal gas in this effective potential. Therefore, the solution can be constructed by solving the one-particle Schrödinger equation whose potential is the right side of Eq. (51), and calculating the densities from the associated form (52) self-consistently,

$$n_\alpha(\mathbf{r}) = \langle\mathbf{r}|(e^{\beta[(p^2/2m_\alpha)+\hat{V}_\alpha-\mu_\alpha]}+1)^{-1}|\mathbf{r}\rangle = \sum_i (e^{\beta(\epsilon_{i\alpha}-\mu_\alpha)}+1)^{-1}|\psi_i(\mathbf{r})|^2. \tag{54}$$

This avoids the difficult problem of finding the functional $\mathcal{V}_\alpha^{(0)}(\mathbf{r}|n)$ but at the cost of having to solve a set of self-consistent Schrödinger equations.

Consider instead an approximate evaluation of the potential $\mathcal{V}_\alpha^{(0)}(\mathbf{r}|n)$ in terms of an effective quantum potential $U_\alpha(\mathbf{r})$ defined by

$$n_\alpha(\mathbf{r}) \equiv \int \frac{d\mathbf{p}}{(2\pi\hbar)^3}(e^{\beta[(p^2/2m_\alpha)+U_\alpha(\mathbf{r})-\mu_\alpha]}+1)^{-1} = \langle\mathbf{r}|(e^{\beta[(\hat{p}^2/2m_\alpha)+\hat{\mathcal{V}}_\alpha^{(0)}-\mu_\alpha]}+1)^{-1}|\mathbf{r}\rangle. \tag{55}$$

The first equality is similar to a finite-temperature Thomas-Fermi representation, with a local chemical potential given by $\mu_\alpha(\mathbf{r})=\mu_\alpha-U_\alpha(\mathbf{r})$. An important difference discussed below is that $U_\alpha(\mathbf{r})\neq V_\alpha(\mathbf{r})$. The functional relationship of $n_\alpha(\mathbf{r})$ to $\mu_\alpha(\mathbf{r})$ and hence to $U_\alpha(\mathbf{r})$ is that for an ideal gas and is well known. The second equality of Eq. (55) defines the semi-classical potential $U_\alpha(\mathbf{r}|\mathcal{V}_\alpha^{(0)})$ as a functional of $\mathcal{V}_\alpha^{(0)}$. This relationship of $U_\alpha(\mathbf{r}|\mathcal{V}_\alpha^{(0)})$ to $\mathcal{V}_\alpha^{(0)}$ is more difficult to unfold. However, it is straightforward to discover it for weak coupling of the system to the perturbing potential. The analysis is similar to the derivation of the Kelbg potential and will not be repeated here. Formally make the replacement $\hat{\mathcal{V}}_\alpha^{(0)} \to \lambda\hat{\mathcal{V}}_\alpha^{(0)}$ in Eq. (55) with the corresponding dependence on λ inherited by $U_\alpha(\mathbf{r})$. Then perform the expansion of $U_\alpha(\mathbf{r})$ to first order in λ, setting $\lambda=1$ at the end, to get [44]

$$U_\alpha(\mathbf{r}) \to \int d\mathbf{r}'\,\pi_\alpha(\mathbf{r}-\mathbf{r}')\mathcal{V}_\alpha^{(0)}(\mathbf{r}'), \tag{56}$$

where $\pi_\alpha(\mathbf{r},\mathbf{r}')$ is the well-known static linear polarization function in the random-phase approximation,

$$\pi_\alpha(\mathbf{r}) = (2\pi)^{-3}\int d\mathbf{r}\; e^{i\mathbf{k}\cdot\mathbf{r}}\tilde{\pi}_\alpha(k), \tag{57}$$

$$\tilde{\pi}_\alpha(k) = \frac{\partial\mu_\alpha}{\partial n_\alpha}\int \frac{d\mathbf{p}}{(2\pi\hbar)^3}\frac{F_\alpha(\mathbf{p}-\hbar\mathbf{k})-F_\alpha(\mathbf{p})}{p^2-(\mathbf{p}-\hbar\mathbf{k})^2}, \tag{58}$$

containing the Fermi distribution

$$F_\alpha(p) = (e^{\beta[(p^2/2m_\alpha)-\mu_\alpha]} + 1)^{-1}. \tag{59}$$

In this approximation, the functional relationship between the density and the potential is now known,

$$n_i(\mathbf{r}) \equiv \int \frac{d\mathbf{p}}{(2\pi\hbar)^3}(e^{\beta[(p^2/2m_i)+\int d\mathbf{r}'\pi(\mathbf{r}-\mathbf{r}')\mathcal{V}_i^{(0)}(\mathbf{r}')-\mu_i]} + 1)^{-1}. \tag{60}$$

Now it is straightforward to improve these results by substitution of Eq. (51) into the right side of Eq. (60), which gives a generalization of the Thomas-Fermi approximation to include strong-coupling effects. However, even if $F_{\mathrm{xc}}(\{n\})$ is neglected, the result is the Thomas-Fermi approximation in terms of the potential

$$\overline{V}_\alpha(\mathbf{r}) = \int d\mathbf{r}'\,\pi_\alpha(\mathbf{r}-\mathbf{r}')V_\alpha(\mathbf{r}') \tag{61}$$

rather than the bare potential $V_\alpha(\mathbf{r})$, which has short-ranged divergences for opposite charge interactions. The result here in terms of the *nonlocal effective quantum potential* appears to be a new one that cures some of the well-known problems of the "local approximation" Thomas-Fermi theory. As indicated below, $\overline{V}_\alpha(\mathbf{r})$ becomes just the Kelbg potential in the nondegenerate limit. The result (60) with Eq. (51) is a nonlinear integral equation for the density, including both *strong-coupling and degeneracy effects.* There is no longer any need to solve the Kohn-Sham equations, and the problem is one of purely classical analysis.

It is instructive to consider the nondegenerate limit. In that case, the polarization function is evaluated using $F_0(p) \to e^{-\beta[(p^2/2m_\alpha)-\mu_\alpha]}$. Furthermore, Eq. (60) simplifies to

$$n_\alpha(\mathbf{r}) = n_\alpha e^{-\beta U_\alpha(\mathbf{r})}, \tag{62}$$

$$\mathcal{V}_\alpha^{(0)}(\mathbf{r}') = \int d\mathbf{r}'\,\pi_\alpha^{-1}(\mathbf{r}-\mathbf{r}')U_\alpha(\mathbf{r}'). \tag{63}$$

Use of these in the DFT equation (51) gives the closed equation for the densities,

$$\ln\frac{n_\alpha(\mathbf{r})}{n_\alpha} = -\beta\overline{V}_\alpha(\mathbf{r}) - \beta\sum_\sigma \int d\mathbf{r}d\mathbf{r}'\,\overline{V}_{\alpha\sigma}(\mathbf{r}-\mathbf{r}')n_\sigma(\mathbf{r}') + \int d\mathbf{r}'\,\pi_\alpha(\mathbf{r}-\mathbf{r}')\frac{\delta F_{\mathrm{xc}}(\{n\})}{\delta n_\alpha(\mathbf{r}')}. \tag{64}$$

The potentials $\overline{V}_\alpha(\mathbf{r})$ and $\overline{V}_{\alpha\sigma}(\mathbf{r}-\mathbf{r}')$ are "regularized" by the polarization function, e.g.,

$$\overline{V}_\alpha(\mathbf{r}) = \int d\mathbf{r}'\,\pi_\alpha(\mathbf{r}-\mathbf{r}')V_\alpha(\mathbf{r}'). \tag{65}$$

It is possible to show [46] that in this *nondegenerate limit* $\overline{V}_\alpha(\mathbf{r})$ *is just the original Kelbg potential*, Eq. (4). Therefore, in the weak-coupling limit where $F_{\mathrm{xc}}(\{n\})$ can be neglected, Eq. (64) becomes the usual Boltzmann-Poisson equation with effective quantum potentials given by the Kelbg potential (4).

In summary, DFT applications can be performed in a semiclassical form without solving the Kohn-Sham equations by introducing effective quantum potentials. This can be done in a weak-coupling approximation similar to that first described by Kelbg and yields a closed analytical result (4). Based on the results of the above analysis, it can be expected that this approach can be extended by incorporating as well effects of degeneracy by using for the density Eq. (52) instead of Eq. (62). Furthermore, by using *improved quantum pair potentials*—along the lines of the improved Kelbg potentials discussed in the previous sections—an accurate treatment of the pair problem is achieved, laying the foundation for advancing DFT to the regime of strong coupling.

VII. CONCLUSION

In this work, we presented an analysis of generalized quantum pair potentials. Extending the work of Kelbg and others, we investigated in detail *effective off-diagonal and diagonal quantum pair potentials* for a correlated hydrogen plasma including spin effects. We studied the accuracy of these potentials by an extensive comparison with the exact solutions of the Bloch equation. Further, we proceeded to an analysis of *improved diagonal quantum pair potentials* by correcting the value of the Kelbg potential at zero particle separation. Excellent agreement with the exact solutions of the two-particle Bloch equations could be achieved with the help of a single temperature-dependent fit parameter for which an accurate analytical Padé formula was presented. This lead to significantly improved diagonal pair potentials compared to the original Kelbg potential. Moreover, these potentials are explicitly spin-dependent and retain the advantage of a closed analytical expression.

These potentials have been applied in path integral Monte Carlo and "semiclassical" molecular-dynamics simulations of dense hydrogen and were found to give accurate results over a wide range of parameters. One important conclusion, of relevance to PIMC simulations, is that the off-diagonal potential gives essentially more accurate results (or more rapid convergence) than its diagonal limit; quantitative estimates have been provided.

Furthermore, we have demonstrated that the spin-dependent improved diagonal potentials are of high use for "semiclassical" molecular-dynamics simulations of partially ionized plasmas. Our analysis revealed that with these potentials, one can successfully simulate dense hydrogen up to moderate coupling and degeneracy, from the fully ionized to

the partially ionized regime. The present potentials allow us to correctly model dense plasmas up to temperatures as low as the molecular binding energy. Further improvements are posible, including the description of molecular hydrogen, but they require the inclusion of three-particle and four-particle correlations and exchange effects beyond the two-particle level.

Finally, an intimate relation of the quantum potentials to density-functional theory has been explored that allows for DFT calculations without the need to solve the Kohn-Sham equations.

ACKNOWLEDGMENTS

We acknowledge stimulating discussions with V. Filinov, W. D. Kraeft, D. Kremp, and M. Schlanges. M.B. gratefully acknowledges the hospitality of the Physics Department of the University of Florida. This work was supported by the Deutsche Forschungsgemeinschaft (BO-1366/2), the National Science Foundation and the Department of Energy (Grants No. DE-FG03-98DP00218 and No. DE-FG02ER54677), as well as by grants for CPU time at the NIC Jülich and the Rostock Linux-Cluster "Fermion."

[1] A. Filinov, M. Bonitz, and W. Ebeling, J. Phys. A **36**, 5957 (2003).
[2] *Strongly Coupled Coulomb Systems*, edited by G. Kalman (Plenum, N.Y., 1998).
[3] *Proceedings of the International Conference on Strongly Coupled Plasmas*, edited by W. D. Kraeft and M. Schlanges (World Scientific, Singapore, 1996).
[4] W. D. Kraeft, D. Kremp, W. Ebeling, and G. Röpke, *Quantum Statistics of Charged Particle Systems* (Akademie-Verlag, Berlin, 1986).
[5] M. Bonitz, *Quantum Kinetic Theory* (B.G. Teubner, Stuttgart/Leipzig, 1998).
[6] *Proceedings of the 10th International Workshop on the Physics of Nonideal Plasmas*, edited by H. Haberland, M. Schlanges, and W. Ebeling [Contrib. Plasma Phys. **41**, No. 2–3 (2001)].
[7] *Progress in Nonequilibrium Greens Functions*, edited by M. Bonitz (World Scientific, Singapore, 2000).
[8] L. B. Da Silva *et al.*, Phys. Rev. Lett. **78**, 483 (1997).
[9] S. T. Weir, A. C. Mitchell, and W. J. Nellis, Phys. Rev. Lett. **76**, 1860 (1996).
[10] G. E. Norman, and A. N. Starostin, Teplofiz. Vys. Temp. **6**, 410 (1968); [Sov. Phys. High Temp. **6**, 394 (1968)]; **8**, 381 (1970); [**8**, 431 (1970)].
[11] P. Haronska, D. Kremp, and M. Schlanges, Wiss. Z. Universität Rostock **98**, 1 (1987).
[12] D. Saumon and G. Chabrier, Phys. Rev. A **44**, 5122 (1991).
[13] M. Schlanges, M. Bonitz, and A. Tschttschjan, Contrib. Plasma Phys. **35**, 109 (1995).
[14] D. Beule *et al.*, Phys. Rev. B **59**, 14177 (1999); Contrib. Plasma Phys. **39**, 21 (1999)
[15] V. S. Filinov, V. E. Fortov, M. Bonitz, and P. R. Levashov, JETP Lett. **74**, 384 (2001) [Pis'ma Zh. Eksp. Teor. Fiz. **74**, 422 (2001)].
[16] W. Ebeling, W. D. Kraeft, and D. Kremp, *Theory of Bound States and Ionization Equilibrium in Plasmas and Solids* (Akademie-Verlag, Berlin, 1976) (Russian Translation Mir, Moscow, 1979).
[17] W. R. Magro, D. M. Ceperley, C. Pierleoni, and B. Bernu, Phys. Rev. Lett. **76**, 1240 (1996).
[18] B. Militzer and D. M. Ceperley, Phys. Rev. E **63**, 066404 (2001).
[19] S. A. Trigger, W. Ebeling, V. S. Filinov, V. E. Fortov, and M. Bonitz, JETP **96**, 465 (2003).
[20] V. S. Filinov, M. Bonitz, W. Ebeling, and V. E. Fortov, Plasma Phys. Controlled Fusion **43**, 743 (2001).
[21] D. Klakow, C. Toepffer, and P.-G. Reinhard, Phys. Lett. A **192**, 55 (1994); J. Chem. Phys. **101**, 10 766 (1994).
[22] V. Golubnychiy, M. Bonitz, D. Kremp, and M. Schlanges, Phys. Rev. E **64**, 016409 (2001).
[23] For completeness, we mention interesting concepts of quantum MD, such as wave packet MD [21] and Wigner function MD [24], which are, however, beyond the scope of this paper.
[24] V. S. Filinov, P. Thomas, I. Varga, T. Meier, M. Bonitz, V. E. Fortov, and S. W. Koch, Phys. Rev. B **65**, 165124 (2002).
[25] G. Kelbg, Ann. Phys. (Leipzig) **12**, 219 (1963); **13**, 354 (1963); **14**, 394 (1964).
[26] C. Deutsch, Phys. Lett. **60A**, 317 (1977).
[27] F. J. Rogers, Phys. Rev. A **23**, 1008 (1981).
[28] M.-M. Gombert, H. Minoo, and C. Deutsch, Phys. Rev. A **29**, 940 (1984).
[29] F. Perrot and M. W. C. Dharma-wardana, Phys. Rev. B **62**, 16536 (2000).
[30] M.-M. Gombert and H. Minoo, Contrib. Plasma Phys. **29**, 355 (1989).
[31] H. Wagenknecht, W. Ebeling, and A. Förster, Contrib. Plasma Phys. **41**, 15 (2001).
[32] R. G. Storer, J. Math. Phys. **9**, 964 (1968); A. D. Klemm and R. G. Storer, Aust. J. Phys. **26**, 43 (1973).
[33] A. A. Barker, J. Chem. Phys. **55**, 1751 (1971).
[34] B. Devies and R. G. Storer, Phys. Rev. **171**, 150 (1968).
[35] K. Rodhe, G. Kelbg, and W. Ebeling, Ann. Phys. (Leipzig) **22**, 1 (1968).
[36] M.-M. Gombert, Phys. Rev. E **66**, 066407 (2002).
[37] D. M. Ceperley, Rev. Mod. Phys. **65**, 279 (1995).
[38] H. Kleinert, *Path Integrals in Quantum Mechanics, Statistics and Polymer Physics*, 2nd ed. (World Scientific, Singapore, 1995).
[39] H. Kleinert, Phys. Rev. D **57**, 2264 (1998).
[40] Since, in this case, individual electrons do not change their spin projection, no exchange processes occur during collisions. This allows us to treat the electrons with opposite spin projection as distinguishable particles and to neglect exchange contributions to the pair potentials. In contrast, in the scattering of two electrons with the same spin projection, exchange does take place, which is taken into account by the potential (14). For a discussion of this question, see C. Cohen-Tannoudji, B.

Diu, and F. Laloe, *Quantum Mechanics* (John Wiley, N.Y., 1977), Vol. 2, Chap. 14.
[41] B. Militzer, Ph.D. thesis, University of Illinois, 2000.
[42] More details of the MD simulations are given in V. Golubnychiy, Ph.D. thesis, Kiel University, 2004.
[43] N. D Mermin, Phys. Rev. **137**, A1441 (1965).
[44] L. Zogaib and J. Dufty (unpublished).
[45] W. Kohn and L. Sham, Phys. Rev. **140**, A1133 (1965).
[46] J. W. Dufty (unpublished).